Electroweak Baryogenesis via Scalar Baryon Number Transport

Thesis by

Eric R. Westphal

In Partial Fulfillment of the Requirements

for the Degree of

Doctor of Philosophy

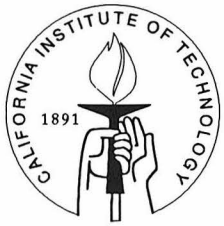

California Institute of Technology

Pasadena, California

1998

(Submitted March 16, 1998)

Acknowledgements

It's my pleasure to thank my collaborators, Krishna Rajagopal and Hooman Davoudiasl, for all the great ideas, inspiration, and frustration which made this thesis possible, and my advisor, John Preskill, for his mentorship. I would also like to thank Sergey Cherkis, Martin Gremm, Anton Kapustin, and Iain and Susan Stewart for enjoyable times and conversations. My family filled my breaks from physics with much-appreciated love and fun, if not relaxation.

Abstract

The study of baryogenesis introduces a new datum in the study of physics beyond the Standard Model. Some physics relevant to baryogenesis is reviewed. Electroweak baryogenesis due to scalar particles (such as squarks) possessing baryon number is estimated and found to be considerable within a broad and plausible range of parameter values. Transport properties of squarks in the electroweak plasma are found to support this conclusion. If baryonic scalars are discovered in physics beyond the Standard Model, these results will be useful in determining whether they are consistent with cosmological observations.

Contents

List of Figures

List of Tables

Chapter 1 Introduction

As particle physics experiments probe ever smaller scales in the quest for the fundamental laws of physics, they become ever more expensive and time-consuming and the amount of relevant experimental observation becomes ever more sparse. Indeed, observations of new physics has slowed to a trickle, all but halting progress in fundamental physics (aside from within essentially speculative areas). It is a fact of paramount importance that the progress of theory is inextricably linked with the progress of experiment. It is crucial to recognize and to exploit this link in order to progress.

One recognition of this link is the principle of integration. Integration, the principle that all knowledge must be noncontradictorily related to form a unified whole, is the dynamo of science [1, 2], converting the observations of experiment into conceptual understanding. Existence exists as a whole, but our consciousness of it and the knowledge we form based upon it is due to contact with only limited aspects of it. If our knowledge is to be true, it must reflect these metaphysical facts; the principle of integration implements this injunction. Any observations bearing on a given theory must be related to it.

Many of the awesome achievements in the rich history of physics were feats of integration: Isaac Newton's relation between the seemingly different motions of heavenly and earthly bodies resulted in his universal laws of motion and gravitation [3]. Einstein united the previously distinct theories of electromagnetism, gravitation, and mechanics into a general theory of relativity encompassing them all [4]. Hans Bethe brought together astronomical observations of the composition of stars and physical observations of nuclear collisions with the theory of quantum mechanics to explain the evolution of stars, thereby improving both astronomical and nuclear theoretical knowledge. These integrations have in common the inclusion of the very large (on an astronomical scale, usually involving astronomical observation) with the very small

(the human scale down to the nuclear scale).

A theory of baryogenesis would also be just such an integration. Such a theory seeks to relate the abundance of matter (and lack of antimatter) observed in the universe, which is a property of the universe on the largest of scales, to particle physics at a subnuclear scale. Such an integration introduces a new and distinctive datum (cosmological) to the study of high-energy physics, where relevant data are difficult to come by. When experiments have nailed down relevant particle properties and the analysis of the electroweak plasma has been refined to the point that a specific baryogenesis scenario can be identified conclusively as responsible for the observed baryon asymmetry, baryogenesis will have matured. It will have integrated an immense set of data on all scales, including countless accelerator events, nuclear and sub-nuclear, and countless astronomical observations. This is the motivation for the study of baryogenesis and its place in modern physics.

For now, the study of baryogenesis is in its adolescence. Baryogenesis is problematic for the Standard Model of particle interactions which serves so well to understand all of the observations of high-energy events in particle colliders. Standard Model physics in the context of the Big Bang simply cannot produce nearly the amount of baryonic matter that is observed in the universe. Therefore, the study of plausible extensions of the Standard Model in the light of baryogenesis may serve to support or rule them out. As the next generation of colliders comes on-line, the input of baryogenesis will become increasingly important in the interpretation of any new physics. Baryogenesis will have come of age.

I cover the essential background physics and cosmology crucial to the study of baryogenesis in Chapter 2. In particular, I discuss Sakharov's conditions for baryogenesis, sphalerons, the properties of the electroweak phase transition, CP violation, and cosmological measurement of the baryon number density. Chapter 3 briefly reviews other work in baryogenesis. In Chapter 4, I cover the main work I have done in the field, the scalar baryon number transport mechanism, and in Chapter 5, I find the diffusion constant for squarks which is necessary to gain quantitative predictions for the transport mechanism I propose. In Chapter 6, I discuss possibilities for a better

treatment of this transport mechanism and its future.

Chapter 2 Physical and Cosmological Background

2.1 The Sakharov Conditions for Baryogenesis

The fundamental observation giving rise to an interest in baryogenesis is that the universe is seen to be dominated by matter—there doesn't seem to be a substantial amount of antimatter anywhere—and yet the laws of physics are very nearly identical for matter and for antimatter. A physical explanation for the dominance of matter and its abundance must clearly exploit this minute difference—that is, baryogenesis must involve processes that violate the symmetries C and CP between matter and antimatter. Since baryogenesis creates a baryon asymmetry where previously there was none, it must also involve baryon number violating processes. Finally, baryogenesis induces a change in the state of the universe, so the universe must be out of thermal equilibrium during the baryogenesis epoch. These three conditions are due originally to Sakharov [5]. They are necessary conditions for a baryogenesis scenario. In summary, baryogenesis must involve

1. a lack of thermodynamic equilibrium,

2. baryon number violating processes, and

3. C and CP violating processes.

The first condition, that the universe be out of thermal equilibrium, narrows down epochs of the early universe during which baryogenesis could have occurred to just a few possibilities.[1] Following the Big Bang, the universe cooled gradually enough

[1]Two further assumptions are implicit in this discussion: that the universe began in a Big Bang scenario and that there was no initial baryon density or that any initial such density was washed out prior to baryogenesis.

that it remained for the most part very nearly in thermal equilibrium throughout its early history (that is, particle processes occurred at a rate much larger than the Hubble constant). The main exceptions relevant for baryogenesis were during the phase transitions when symmetries in the laws of physics were broken. There were at least three such phase transitions: at the GUT scale, when a GUT symmetry such as $SU(5)$ broke to $SU(3) \times SU(2) \times U(1)$; at the electroweak scale, when $SU(2) \times U(1)$ broke to the electromagnetic and weak interactions; and at the chiral symmetry breaking scale. The final phase transition, when the chiral symmetry was broken (at a temperature of a few hundred MeV), was already too late: at these well-explored energies, there are no baryon number violating processes in equilibrium. Indeed, there are no significant baryon number violating processes in equilibrium after the electroweak phase transition. However, before the electroweak phase transition, there were sphaleron processes (discussed below in Section 2.3) which do violate baryon number. These baryon number violating processes dropped out of thermal equilibrium during the electroweak phase transition, identifying it as prime territory to look for baryogenesis.

During the time between the GUT phase transition and the electroweak phase transition, the sphaleron processes were in thermal equilibrium along with all other particle processes. This means that any nonzero baryon density produced before the electroweak phase transition would be washed out by the sphalerons (but only if baryon minus lepton number $B - L$ is zero; note that $B - L$ is conserved in minimal $SU(5)$). Furthermore, inflation would also likely wipe out any baryon density created during the GUT phase transition. Nevertheless, baryogenesis occurring at the GUT phase transition has been studied [6]. However, because GUT energies will be inaccessible to experiments performed any time soon, I will not consider GUT baryogenesis in any depth.

The study of electroweak baryogenesis is very attractive because the relevent energies will be within reach of the next generation of particle accelerators. It is also the "last chance" for baryogenesis to occur as there are no B-violating processes in thermal equilibrium at temperatures below the phase transition temperature. My

research in baryogenesis has focused on electroweak baryogenesis. There are two distinct categories of electroweak baryogenesis: baryogenesis resulting from topological defects [7] and charge transport baryogenesis. My research has been on charge transport baryogenesis.

Clearly, the properties of the electroweak phase transition are crucial to any study of electroweak baryogenesis. I will describe the relevant properties and what is known about them in the next section. In Section 2.3, I will discuss the essentials of the B-violating processes occurring during the phase transition—the sphalerons. Finally, in Section 2.4, I will discuss relevant sources of CP violation at the scale of the phase transition. I will finish this chapter by discussing in Section 2.5 the astrophysical data to be integrated with particle theory.

2.2 The Electroweak Phase Transition

In this section, I discuss relevant characteristics of the electroweak phase transition and briefly mention how these characteristics are computed. The phase transition is a transition of the Higgs field from a zero expectation value to a finite expectation value, and the character of this transition is determined by the properties of the Higgs field along with those of the other fields which are present at the time of the phase transition. The exact characteristics of the phase transition are not well known because the Higgs mass and multiplicity are not known. However, bounds on the Higgs mass and other considerations will limit the possible properties of the phase transition enough for the study of baryogenesis to proceed.

In order for electroweak baryogenesis to be tenable, the electroweak phase transition must be first order. Simply, in a first order phase transition, an order parameter (in this case the expectation value of the Higgs field) jumps discontinuously as the temperature changes. As the phase transition temperature is crossed, bubbles nucleate within which the order parameter takes on its new parameter (though the order parameter will vary smoothly across the wall of the bubble). The bubbles expand and collide, converting all of space to the new phase. During the time of the bubble

nucleation, the system is out of thermal equilibrium—one of Sakharov's requirements is fulfilled. The other possibility is that the phase transition is second order, in which case the order parameter changes continuously and with infinite correlation length. No bubbles are nucleated, and the system does not leave thermal equilibrium. It is crucial for baryogenesis that the phase transition be first order. If it is first order, then in order to perform a quantitative analysis of baryogenesis, it is crucial to determine dynamic properties of the phase transition such as the velocity of the expanding bubble walls and the wall thickness in addition to static properties such as the temperature T_c of the phase transition and its order parameter.

Static properties of the phase transition, in particular the order of the phase transition and its order parameter and the critical temperature, can be calculated by studying the effective potential of the Standard Model (plus possibly some extension of it) in finite temperature field theory. The approximate finite temperature effective potential (for both the MSM and a two-Higgs extension) has been studied at one loop [8, 9], with two-loop corrections [10], and on the lattice [11]. The phase transition is more strongly first order for a two Higgs model, but it would probably still be acceptably strong even for the Standard Model if the Higgs is light enough. The critical temperature T_c seems to lie somewhere around 100 GeV to 150 GeV and the order parameter is somewhere between 90 GeV and 250 GeV, depending on the Higgs mass [12].

Dynamic properties of the phase transition are studied numerically by solving a differential equation for the Higgs field in a viscous environment. The wall velocity and thickness are not yet well constrained. Estimates range from $10/T$ to $100/T$ for the thickness of the wall [9, 13] and from 0.02 [9] to 0.8 [13, 14] for the wall velocity.

A stronger phase transition, favorable to baryogenesis, would require multiple or light Higgs. Multiple Higgs fields further strengthen baryogenesis by allowing for more CP violation than is in the Standard Model, as discussed in Section 2.4. If the Higgs exists, it should be discovered within the next decade. Experimental detection of Higgs and determination of their number and masses would significantly improve our understanding of the electroweak phase transition and its properties. However,

further simulations would also be useful in determining its properties, especially the dynamical ones.

2.3 Sphalerons

At temperatures above the critical temperature, there are baryon number violating processes called sphalerons in thermal equilibrium. Below the critical temperature, when the electroweak symmetry is broken, the sphalerons are suppressed. This situation is ideal for baryogenesis: during the phase transition, if baryons gather inside the bubbles of broken phase, where sphalerons are suppressed, and antibaryons gather outside the bubbles of broken phase, where sphalerons are active, then the antibaryons will be washed out while the baryons remain, resulting in baryogenesis. This is the basis of the scalar baryon number transport mechanism which I present in Chapter 4, and similar baryogenesis scenarios are termed "charge transport scenarios." In this section, I discuss the essentials of the sphaleron processes.

A sphaleron is a type of nonperturbative process in field theory [15]. To understand them, it is useful to make an analogy with a pendulum. There are two classes of motions for a classical pendulum, both oscillatory. One class, for small energies $E < 2mgl$, involves oscillations about the configuration of minimum energy; within this class, motions can be described by perturbation theory about a harmonic oscillator solution, with the perturbation series converging quickly for small energies and not so well for energies approaching the critical energy. The other class, for large energies $E > 2mgl$, involves oscillations in which the pendulum rotates completely about its pivot point; within this class, motions can be described by perturbation theory about a free particle solution, with the perturbation series converging quickly for large energies and not so well again for energies approaching the critical energy. From the perspective of the class of low-energy motions, these motions are non-perturbative. There is also a third type of motion, that in which the oscillator has the critical energy $E = 2mgl$ (it turns out that the solution for this energy is known analytically).

A further property of these classes of motion distinguishes them. Because all

pendulum motions are periodic, the motion is completely described by one period of the motion. In the configuration space of the pendulum, this will correspond to a loop. For trajectories in the low-energy class, this loop is contractible to a point in the configuration space; but for the high-energy class, the loop is *non-contractible.* The possibility of these large motions is a result of the nontrivial topology of the configuration space (which is a circle in θ). One could also put the pendulum pivot on a screw rather than on a pin, so that there is an infinitude of degenerate minimum-energy configurations, which may be labeled by the set of integers. Small motions (corresponding to a contractible loop) oscillate about one minimum-energy configuration (they correspond to a single integer) and large motions (corresponding to a non-contractible loop) interpolate between one minimum-energy configuration and another (corresponding to a change in integer—the winding number).

A quantum mechanical pendulum displays similar behavior. However, if the pendulum is initially confined to a ground state corresponding to a single integer, it will now have a finite probability of tunnelling to another of its degenerate ground states. Thus there are two ways for a quantum pendulum to go from one ground state to another: via a large motion or via tunnelling. The true time-independent ground states correspond to superpositions in which the pendulum has an equal probability of being found in the ground state corresponding to any integer.

With this picture in mind, it is now easy to understand some nonperturbative phenomena in field theory. The essential difference here is that in field theory, the configuration space (corresponding to all possible functional spacetime dependencies of all the fields, up to gauge transformations) is infinite-dimensional. Nevertheless, in some field theories, trajectories have been found [15] which begin and end on vacuum configurations and which are not smoothly deformable (contractible) to a trivial trajectory (these are the analogs of the large motions of the pendulum). This is again a reflection of a nontrivial topology of the field configuration space. The integer labeling the vacuua (minimum energy configurations) in this case is the Chern-Simons number of the field configuration. Nonabelian gauge theories display such field configurations, with the gauge field corresponding to the pendulum. Instances

in which the vacuum tunnels to a different vacuum are called instantons.

In the electroweak theory, there is a minimum energy (analogous to the critical energy of the pendulum) which a gauge field trajectory must have in order to surmount the potential barrier separating vacua (as opposed to tunneling through it). The field configuration with this energy, at the top of the barrier, is called a sphaleron. The sphaleron configuration is unstable, collapsing toward the vacuum configurations on either side of the barrier. The sphaleron energy was computed to be nearly 10 TeV [12]. The sphaleron rate has been estimated for temperatures below the phase transition temperature when the gauge symmetry is broken, and was found to be appreciable near the phase transition temperature if the Higgs is heavier than 50 GeV (corresponding to a weak phase transition) [16]. This is already lower than the experimental bound, indicating that the Standard Model phase transition could be too weak for baryogenesis. Additional scalar matter will strengthen the phase transition [17]. Above the phase transition temperature, in the symmetric phase where the full nonabelian symmetry holds, the sphaleron barrier is lower and dimensional analysis [15] shows that the sphaleron transition rate at a temperature $T > T_c$ is

$$\Gamma_{sph} \approx \kappa(\alpha_W T)^4 \ . \tag{2.1}$$

Recent work [18] shows that κ is parametrically $\mathcal{O}(\alpha_W)$. The most complete numerical simulations done to date [19] suggest $\kappa = (29 \pm 6)\alpha_W \approx 1$ just above the phase transition.

When fermion fields are present, these topological transitions cause the famous anomaly in their axial current [20]. This is because what was a zero energy state of the fermion in the original vacuum becomes a positive energy state in a neighboring vacuum, and what was a negative energy state (an antifermion) in the original vacuum becomes a zero-energy state in the neighboring vacuum (or vice versa). All the energy levels for the fermion states are shifted up (or down) in this way under the change of vacuum. In the electroweak theory, this results in a violation of B+L [21]. This supplies the baryon number violation necessary for baryogenesis.

2.4 CP Violation at the Electroweak Phase Transition

Having established and discussed the presence of baryon number violating processes during the electroweak phase transition and the out of equilibrium nature of the electroweak phase transition, I now turn to a discussion of CP violating physics at the phase transition. This will complete my survey of the physics fulfilling the Sakharov conditions at the electroweak phase transition.

In a generic baryogenesis scenario (already briefly mentioned), the out of equilibrium condition involves bubbles of broken phase expanding within the symmetric phase. Since the sphaleron processes are active outside the bubbles but are inactive inside, if baryons gather inside the bubbles where they are protected from the sphalerons and antibaryons remain outside, baryogenesis will result. Clearly, the physics which results in the separation of baryons and antibaryons must involve a CP violating interaction with the bubble wall. (C is violated maximally in the Standard Model, so I take it for granted henceforth.) Microscopically, this means that the baryons must interact with the Higgs field in a CP violating manner.

In the Standard Model, the only baryonic matter is the quarks. The interaction of the quarks with the Higgs field (which has taken on a vacuum expectation value at zero temperature) gives them masses and flavor-changing interactions with the W boson (parametrized by the Cabbibo-Kobayashi-Maskawa matrix) and Higgs boson. Flavor changing processes involving all three generations of quarks are CP violating; the CP violation in the Standard Model is weak because it exists only for these three-generation flavor-changing processes.

At the electroweak phase transition, the changing expectation value of the Higgs field across the bubble wall gives the quarks masses which vary across the bubble wall. This and interactions with the particles swept along with the wall will result in a partial reflection of the quarks as they impinge upon the wall. CP violating interactions with the W bosons and Higgs bosons in the plasma will result in differing coefficients of reflection from the wall for particles and antiparticles. In the next

chapter, I review the Standard Model baryogenesis scenario [22] and how it was shown [23] that it produces only a negligible baryon density, essentially due to the weakness of the CP violation in the Standard Model (as mentioned in the previous section, another problem with the Standard Model is that it does not produce a strong phase transition, leaving the baryons injected into the broken phase inside the bubbles somewhat vulnerable to sphaleron processes).

Given the failure of the Standard Model to account for the baryon asymmetry of the universe, there is good motivation to explore minimal extensions to the Standard Model at the electroweak scale that include enough CP violation to produce the observed baryon asymmetry. The minimal extension with the best motivation in other contexts (e.g., for solution of the hierarchy problem) is the Minimal Supersymmetric Standard Model (MSSM), so it is certainly natural to explore baryogenesis under this scenario. I will briefly review some existing approaches to MSSM baryogenesis [24, 25, 17, 26, 27, 28] in the next chapter.

The MSSM contains more than twice as many particles as the Standard Model, so it is not surprising that it introduces an abundance of new CP violation. Of particular interest is the second Higgs doublet field in the MSSM. With two Higgs fields, there will be CP violation directly in the interaction between the Higgs wall and the baryonic matter, greatly strengthening the effect of the CP violation in baryogenesis. The considerable drawback attendant to introducing this abundance of CP violation is that experimental constraints are weak. CP violation in the MSSM will be discussed at length in Chapter 4 when the scalar baryon number transport mechanism is introduced.

2.5 Cosmological Observations

The most immediate observation that the universe is baryon-asymmetric is that, rather than annihilating, when you stub your toe it merely throbs with pain. On Earth, the only antimatter is manmade. Neil Armstrong and the Pioneer probes dramatically established that there is no substantial antimatter anywhere else in the

solar system. The universe is at least locally baryon asymmetric [29].

Further astronomical observations establish that there is no substantial antimatter elsewhere in the visible universe [30]. The antimatter component of cosmic rays is composed primarily of secondaries. This indicates that the galaxy and probably the local cluster are made overwhelmingly of matter. The absence of the significant γ-ray flux which would result from matter-antimatter annihilation in the intergalactic medium is further evidence that clusters of galaxies are baryon asymmetric. There's little evidence one way or the other on the scale of superclusters, however.

If there were no baryogenesis, nucleons and antinucleons would remain in chemical equilibrium until a temperature of only about 20 MeV. They would have the proper density at a temperature of about 40 MeV. However, the horizon at this time would have been only a small fraction of a solar mass, so even if a mechanism were known for separating chunks of matter from antimatter, it could not isolate enough to account for the cosmological asymmetry [29]. Baryogenesis seems to be the only possible mechanism for generating the observed asymmetry.

The baryon density n_B is usually quoted as a fraction of the total (entropy) density s because n_B/s is independent of the expansion of the universe (so long as entropy is not produced). This quantity, the output of baryogenesis, is one of the primary inputs for nucleosynthesis, one of the most successful theories in cosmology. In order to predict the observed light element abundances, nucleosynthesis requires a baryon to entropy ratio of $(4-7)\times 10^{-11}$ [31]. This is the datum which a theory of baryogenesis must match.

Chapter 3 Other Scenarios for Electroweak Baryogenesis

The work of Sakharov [5], which I reviewed in the previous chapter, introduced the subject of baryogenesis as a subject worthy of scientific study. Because its CP violation is so weak, it seemed unlikely that the Standard Model could produce significant baryogenesis. So baryogenesis was perhaps first seriously considered in the context of Grand Unified Theories (see [29] for a brief but more complete review). Briefly, if a GUT possesses $B - L$ violating interactions (the minimal GUT, $SU(5)$, does not), usually appearing in the form of GUT leptoquarks, then sphaleron transitions below the GUT scale will convert a nonzero $B - L$ into a nonzero B. Problems abound for GUT baryogenesis: $B - L$ must be a good symmetry at low temperatures, but broken at the GUT scale; and generally, inflation will wipe out any GUT baryon asymmetry. The most significant problem with GUT baryogenesis is that its parameters are largely unconstrained and unlikely to become more constrained in the near future. I will not consider GUT baryogenesis any further. There are also electroweak baryogenesis mechanisms involving topological defects [7]. These also are quite different from charge transport scenarios as studied in this work and I will not consider them any further.

3.1 Standard Model Baryogenesis and Decoherence

Standard Model baryogenesis and its problems are best illustrated by considering the work of Farrar and Shaposhnikov [22]. Their proposal follows the lines of the generic mechanism discussed in the previous chapter. In brief, it assumes a first order

electroweak phase transition accompanied by bubbles of broken symmetry expanding inside the symmetric background. Quarks in the plasma scatter off the bubbles and are partially transmitted and partially reflected. CP violating interactions between the quarks and the plasma result in more baryons inside the bubbles of broken phase, where they are protected from baryon number violating sphalerons, and more antibaryons in the symmetric phase, where baryon number violating processes are rampant and tend to destroy them.

This mechanism was found to suffer from two difficulties which render inadequate the baryon asymmetry it produces. The first problem is the weakness of the electroweak phase transition in the Minimal Standard Model. This problem is not specific to their model and is corrected if there are more scalars in the theory. The second problem is due to the weakness of the CP violation in the Standard Model. In order for CP violation to influence baryogenesis, quantum mechanical interference must take place between two processes. In the first process, a quark scatters once off the wall, changing flavor in the collision. In the second process, it must scatter three times off the wall, changing flavor each time and hitting each generation, and returning in the same state as the first process. Since it involves flavor changing processes covering all three generations, the amplitude for the second process will contain a CP violating phase. Under interference with the amplitude for the first process, this phase will result in different coefficients of reflection (which are proportional to the squared amplitude) for particles and antiparticles.

This intricate quantum mechanical interference is subject to decoherence due to interactions of the quark with the plasma. In particular, the gluons possess the strongest coupling to the quarks, so the quarks will scatter off the gluons predominantly. Because a collision with a gluon will induce a random phase in the amplitude, the CP violation can become obscured by these decoherence-inducing scatterings if this random phase is comparable to the CP violating phase. Indeed, several groups [23] showed that this is the case. The Standard Model cannot produce a significant baryon asymmetry because its CP violation is too weak to overcome this decoherence.

3.2 Supersymmetric Baryogenesis

MSSM baryogenesis has been studied extensively [24, 32, 26, 27, 28]. Here I will review very briefly the mechanism developed by Huet and Nelson [25] as representative of these scenarios. The Minimal Supersymmetric extension of the Standard Model introduces new CP violating physics as well as new baryonic content (the squarks). In particular, in the quark sector, quarks will obtain masses and CP violating mixings which are space-dependent (the details in the quark case are similar to the squark case as presented in the next chapter). This is in sharp contrast to the Standard Model case, in which the CP violation is constant in space and is due entirely to charged current interactions. The result is that the CP violation in the MSSM is much stronger.

As the bubble walls from the phase transition sweep across the universe, quarks in the plasma will reflect off the Higgs walls just as in the Standard Model case. Top quarks have the strongest coupling to the Higgs, so they will reflect most strongly and will ultimately make the largest contribution to baryogenesis. Due to the CP violating interaction with the bubble wall encoded in the space-dependent mixings, left-handed quarks will have a different reflection coefficient from right-handed anti-quarks (their CP conjugate). As a result, the quarks reflected into the symmetric phase will carry a net $SU(2)$ doublet number. The sphaleron transitions in the symmetric phase, which are a manifestation of the electroweak $SU(2)$ gauge symmetry, will be biased toward reducing this doublet number to achieve chemical equilibrium. Since reducing $SU(2)$ doublet number corresponds to reducing baryon number, the result will be baryogenesis. Again, the particles in the broken phase are protected from the baryon number violating processes. Also, the right-handed quarks and anti-quarks are not $SU(2)$ charged and do not feel the effects of sphalerons. These MSSM mechanisms will be discussed further in contrast to the mechanism proposed in this thesis in the next chapter.

Chapter 4 Scalar Baryon Number Transport

4.1 Description of the Mechanism

In [33], Hooman Davoudiasl, Krishna Rajagopal, and I introduced a new mechanism for generating the BAU at the electroweak phase transition. Our mechanism requires augmenting the Standard Model by the addition of (at least) two baryonic complex scalar fields ϕ_1 and ϕ_2 with masses of $\mathcal{O}(T_c)$. The two fields must be coupled by off-diagonal terms in their (Hermitian) mass-squared matrix M^2 which include a CP violating phase. In this way, we introduce CP violation beyond that in the CKM matrix. Furthermore, we require that M^2 depend upon the Higgs field expectation values so that the mass eigenvalues and eigenstates are different in the symmetric and broken phases. The requirements just sketched can be implemented in a variety of extensions of the Standard Model. Perhaps the most appealing possibility is that ϕ_1 and ϕ_2 are the $SU(2)$ singlet and $SU(2)$ doublet top squarks in a supersymmetric extension of the Standard Model. Another possibility, of interest in light of the recent HERA anomaly [34], is that ϕ_1 and ϕ_2 may be weak-scale leptoquarks whose masses receive contributions from couplings to the Higgs field. We focus on the baryogenesis mechanism rather than on model building; for concreteness, however, we present our mechanism and results taking the ϕ's to be squarks, and defer discussion of other possibilities to Section 4.5 after the mechanism has been detailed.

In a supersymmetric theory, the mass-squared matrix M^2 depends upon $v_1(T)$ and $v_2(T)$, the temperature-dependent expectation values of the two Higgs doublets H_1 and H_2 that give mass to the down- and up-type quarks, respectively. The off-diagonal terms in M^2 are in fact zero in the symmetric phase, where $v_1 = v_2 = 0$. In the broken phase, the off-diagonal terms are complex and therefore CP violating.

We define ϕ_1 and ϕ_2 as the eigenvectors of M^2 in the symmetric phase and note that the mass eigenvectors in the wall and in the broken phase are linear combinations of these symmetric phase eigenvectors.

We will be interested in the reflection and transmission probabilities of ϕ's incident on the wall from the symmetric phase. Because of the CP violating phases in M^2, the probability R_{12} for an incident ϕ_1 to be reflected back into the symmetric phase as a ϕ_2 is not the same as $R_{\overline{12}}$, the probability for an incident antiparticle $\bar{\phi}_1$ to be reflected as a $\bar{\phi}_2$. We will show that this reflection asymmetry $\Delta R \equiv R_{12} - R_{\overline{12}}$ results in a net flux of baryon number from the bubble wall into the symmetric phase, matched by a flux of the opposite sign into the broken phase. Note that the measure of CP violation in the model is the spatial variation of the phase of the off-diagonal terms in M^2. A spatially constant phase can be rotated away by a spacetime-independent unitary transformation on the ϕ_i; hence the phase must vary spatially if ΔR is to be nonzero.

The central observation of this work is that the reflection asymmetry ΔR can be large (approaching 1) over a broad range of incident energies if the phase of the off-diagonal term in M^2 changes by $\mathcal{O}(1)$ as the bubble wall is traversed from the symmetric phase to the broken phase. As already noted, because of the dependence of M^2 on v_1 and v_2, the eigenvalues of M^2 vary within the bubble wall. We assume that the larger of the two eigenvalues in the broken phase is greater than the larger of the two eigenvalues in the symmetric phase. This means that there is in general a range of incident energies E such that in the symmetric phase, both eigenvalues of M^2 are below E^2, while in the broken phase, there is only one eigenvalue below E^2. Therefore, there are two propagating modes with energy E in the symmetric phase and only one in the broken phase. Consider a ϕ_1 incident upon the wall from the symmetric phase with an energy in this range. As it begins to penetrate the wall, it evolves into a linear combination of the position-dependent eigenstates of the matrix M^2. Since only one mode can propagate in the broken phase, there is a position within the wall at which one mode is totally reflected. The reflected mode, upon re-emerging into the symmetric phase, is some linear combination of ϕ_1 and ϕ_2 which includes a

significant ϕ_2 component if there is significant mixing. Another way of understanding what is special about the range of energy under discussion is that at each energy in this range, there is one linear combination of incident ϕ_1 and ϕ_2 that is totally reflected. For this reason, both R_{12} and $R_{\overline{12}}$ are generically large, and ΔR is also large unless the CP violating phase is small. We will refer to this range of incident energies as the "enhanced reflection zone."[1] By comparison, for incident energies above the enhanced reflection zone, for which there are two propagating modes in both the symmetric and broken phases and throughout the bubble wall (so that there is no total reflection), we find that ΔR is nonzero but is generically many orders of magnitude smaller than one. The width in energy of the enhanced reflection zone is comparable to the amount by which the masses change between the two phases; in the example we present, the width of the enhanced reflection zone is 90 GeV. In Section 4.2, we present the parametrization of M^2 appearing in a supersymmetric theory. We then set up the calculation of ΔR, leaving a detailed presentation of the method of calculation to the supplementary Section 4.6. We also evaluate ΔR and explore its dependence on parameters in M^2 in Section 4.2.

Standard Model quarks also have an enhanced reflection zone, as discussed by Farrar and Shaposhnikov [22], although its width is only of order the strange quark mass. The resulting BAU is small [23], essentially because the light quarks have mean free paths much shorter than their Compton wavelengths. We defer to Section 4.4 a discussion of the suppression due to the finite mean free path of the heavy scalars we employ in our mechanism; the suppression is not severe.

In Section 4.3, we integrate ΔR against the appropriate thermal distributions for incident ϕ_1's and ϕ_2's to obtain the baryon number flux injected into the symmetric phase. If the wall velocity v_w is zero, or if the masses of ϕ_1 and ϕ_2 in the symmetric phase are equal, we find that the baryon number flux due to incident ϕ_1's is cancelled by that due to incident ϕ_2's. As long as $v_w \neq 0$ and the masses in the symmetric phase are not degenerate, we obtain a nonzero baryon number flux. The

[1] We will show that for energies in the enhanced reflection zone, scalars incident upon the wall from the broken phase do not yield a reflection asymmetry and hence do not contribute to the BAU.

larger the fraction of the thermal distributions for incident ϕ's lying in the enhanced reflection zone, the larger the baryon number flux will be. The final element in the mechanism involves electroweak baryon number violating processes. These drive the baryon number density in the symmetric phase toward zero. Because they do not act significantly in the broken phase, the final result is a net baryon asymmetry of the universe whose magnitude we estimate in Section 4.4. Our mechanism yields a BAU consistent with observation if the scalars have nondegenerate masses of order T_c in the symmetric phase and if the bubble walls are reasonably thin and slow. We discuss open questions and model implementations in Section 4.5 and note there that an enhanced reflection zone can arise in leptoquark models, and thus is not peculiar to supersymmetric theories.

To close this introduction, we contrast our mechanism with the charge transport mechanism, pioneered by Cohen, Kaplan and Nelson [35, 36], further developed by many authors, and often used to estimate the BAU generated during the electroweak phase transition in supersymmetric theories [25, 17, 26, 27, 28]. Our mechanism can be seen as a modification of the charge transport mechanism. We make explicit comparisons with the results of Huet and Nelson [25] obtained using the charge transport mechanism and find that our mechanism can yield an n_B/s consistent with observation for smaller CP violating phases. The central difference is that in our mechanism, we generate a flux of baryon number into the symmetric phase, whereas in the charge transport mechanism a flux of another quantum number, often left-handed baryon number minus right-handed baryon number, is generated. This axial baryon number can be washed out by QCD processes before it has time to bias electroweak baryon number violating processes [37]. Because our mechanism generates a baryon number flux, it is immune to QCD interference of this kind.[2] This contrast is particularly germane in light of the recent demonstration that the rates for the relevant QCD processes are significantly larger than previously expected [38]. Various authors have

[2]We should note that there are scenarios in which baryogenesis via the generation of an axial baryon number current can be immunized against suppression due to strong sphalerons. One example [25] requires that the left- and right-handed top squarks and the left-handed bottom squark have symmetric phase masses comparable to the temperature while the other squarks are heavier. Another example [38] requires the formation of a squark condensate just above T_c.

noted the possibility that a baryon number flux may be generated, but this has always been assumed to be a small effect. This is in fact true for incident energies such that the number of propagating modes is the same on both sides of the bubble wall. For a generic mass-squared matrix M^2, however, there is a broad region of incident energies in which fewer modes propagate in the broken phase. We observe that this leads to large reflection asymmetries, and consequently to a large baryon number flux into the symmetric phase, yielding an efficient mechanism for generating a BAU consistent with cosmological observations during the electroweak phase transition. We will refer to the electroweak baryogenesis mechanism we propose as the scalar baryon number transport mechanism.

4.2 M^2, ΔR, and the Enhanced Reflection Zone

We begin this section by presenting the parametrization of M^2 appropriate for a supersymmetric theory, when ϕ_1 and ϕ_2 are left- and right-handed top squarks, and then set the stage for the calculation of ΔR. We then describe the dependence of ΔR upon the incident energy and upon parameters in M^2.

As discussed in the introduction, the CP violation that we exploit results from the mixing between two scalars as they traverse the bubble wall separating regions of symmetric and broken phase at the critical temperature T_c. In this background, terms in the potential that couple the baryon number carrying scalars ϕ_i to the Higgs fields H_1 and H_2 give the ϕ_i spacetime–dependent masses and mixings which can be encoded in a 2×2 Hermitian mass matrix. In a supersymmetric theory, the scalars ϕ_i are squarks. Top squarks (stops) are the most promising candidates to play the role we envision for the ϕ_i's because they can be light without violating experimental upper bounds on neutron and electron electric dipole moments (EDMs). Indeed, Cohen, Kaplan, and Nelson have recently advocated supersymmetric models in which CP violating phases are $\mathcal{O}(1)$, but observable EDMs do not arise because the first and second generation squarks have masses in the tens of TeV [39]. Although it is conceivable that the scalar baryon number transport mechanism could be imple-

mented using first or second generation squarks, it seems likely that stops will yield the largest contribution to the BAU. The stop mass matrix M^2 is [40]

$$\begin{pmatrix} \tilde{m}_{tR}^2 + m_t^2 + m_Z^2 \cos 2\beta \left(\frac{2}{3}\sin^2\theta_W\right) & m_t(Ae^{i\varphi_A} + \mu e^{i\varphi_B}\cot\beta) \\ m_t(Ae^{-i\varphi_A} + \mu e^{-i\varphi_B}\cot\beta) & \tilde{m}_{tL}^2 + m_t^2 + m_Z^2 \cos 2\beta \left(\frac{1}{2} - \frac{2}{3}\sin^2\theta_W\right) \end{pmatrix} \tag{4.1}$$

Here, $m_t = \lambda_t v_2$ is the top quark mass, $m_Z^2 = g^2(v_1^2 + v_2^2)/2$ is the Z boson mass squared, $\tilde{m}_{tR}$ is the soft SUSY-breaking mass for the $SU(2)$ singlet stop, $\tilde{m}_{tL}$ is the soft SUSY-breaking mass for the $SU(2)$ doublet stop, $\tan\beta = v_2/v_1$ is the ratio of the Higgs field expectation values, $\mu e^{i\varphi_B}$ is the (complex) mass in the Higgs potential coupling the two Higgs fields, and $Ae^{i\varphi_A}$ is a complex soft SUSY-breaking term. We will see that the scalar baryon number transport mechanism works best if $\tilde{m}_{tL}$ and $\tilde{m}_{tR}$ are both $\mathcal{O}(T_c)$ and differ by about 10-30%. Mass differences of this order can arise due to renormalization group evolution down from some high energy scale at which $\tilde{m}_{tL} = \tilde{m}_{tR}$. Indeed, in the models of Ref. [41], $\tilde{m}_{tL}$ and $\tilde{m}_{tR}$ differ by 20%.

During most of the existence of the expanding bubble, its wall can be treated as flat because its radius of curvature is much larger than its thickness, so the mass matrix will depend only upon one spatial direction. We call this the x direction, with the region of large negative x being the symmetric phase and that of large positive x the broken phase. Both v_1 and v_2 vary across the bubble wall. A complete calculation of these profiles is beyond the scope of this work, although a treatment using the resummed one-loop temperature-dependent effective potential is possible [42]. To simplify calculations, we make a simple choice in terms of a single width parameter, which should capture the essential physics. Following Ref. [26], we choose profiles such that the $v_i(x)$ are x-independent for $x < -w/2$ and $x > w/2$ and are sinusoids for $-w/2 < x < w/2$. That is, we define the profile function

$$p(x) = \begin{cases} 0 & x \le -w/2 \\ \frac{1}{2} + \frac{1}{2}\sin\left(\frac{\pi x}{w}\right) & -w/2 < x < w/2 \\ 1 & x \ge w/2 \end{cases} \tag{4.2}$$

and then for v_1, we take

$$v_1(x) = v_1^0 p(x) \ , \tag{4.3}$$

which varies smoothly from zero in the symmetric phase at $x \to -\infty$ to v_1^0 in the broken phase at $x \to \infty$. The parameter w characterizes the width of the wall separating the two phases. The choice (4.2) is convenient numerically, as it allows us to impose boundary conditions at $x = \pm w/2$ rather than at larger $|x|$.

It is crucial to our mechanism that v_2/v_1 vary across the bubble wall so that the overall phase of the off-diagonal term in M^2 is not constant spatially (in which case it could be rotated away). We take

$$\begin{aligned} v_2(x) &= v_1(x) \tan\beta(x) \\ &= v_1(x) \left[p(x) \tan\bar{\beta} + (1 - p(x)) \tan(\bar{\beta} - \Delta\beta) \right] \end{aligned} \tag{4.4}$$

so that $\tan\beta(x)$ varies from $\tan(\bar{\beta} - \Delta\beta)$ in the symmetric phase to $\tan\bar{\beta}$ in the broken phase. We will take $\tan\bar{\beta} = 2$ in our estimates. Our results do not depend sensitively on this choice. The appropriate choice for v_1^0 in (4.3) is *not* (250 GeV) $\cos\bar{\beta}$, the value it takes at $T = 0$, but rather the value it takes in the broken phase at $T = T_c$. This can be calculated as a function of parameters in specific models, but we will simply use the reasonable estimate $v_1^0 = (2/3)(250 \text{ GeV}) \cos\bar{\beta}$. (Our results also do not depend sensitively on the choice of prefactor.) In order for the baryon asymmetry generated (by any mechanism) during the electroweak phase transition not to be wiped out, $(v_1^0)^2 + (v_2^0)^2$ must be larger than T_c^2. Estimates for $\Delta\beta$ exist in specific models and range from $0.01 - 0.03$ [26, 43] to 0.25 [28], but there are certainly no experimental constraints on this parameter. In order for the overall phase of the off-diagonal terms in M^2 to vary with x, that is, in order for M^2 to introduce CP violating effects, we must have

$$\begin{aligned} \Delta\beta &\neq 0 \\ \Delta\varphi &\equiv \varphi_A - \varphi_B \neq 0 \ . \end{aligned} \tag{4.5}$$

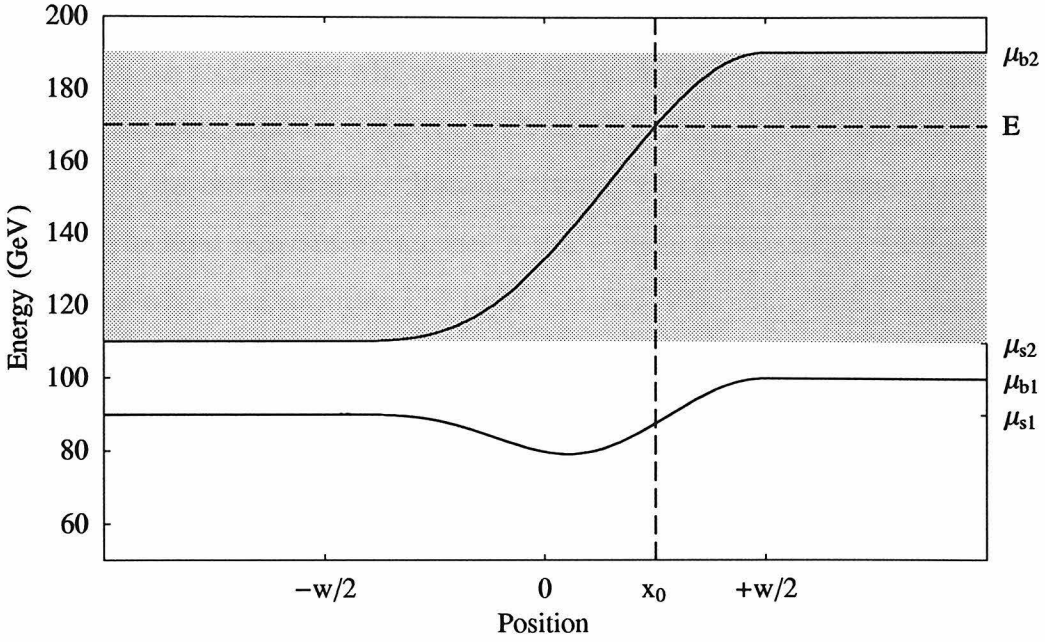

Figure 4.1: Mass eigenvalues as a function of position. The two curves show the square roots of the eigenvalues of M^2, with parameters given in the text, as a function of x. w is the wall width. μ_{s1} and μ_{s2} are the mass eigenvalues in the symmetric phase, and μ_{b1} and μ_{b2} are the mass eigenvalues in the broken phase. For any incident energy in the shaded range $\mu_{s2} < E < \mu_{b2}$, there is a position x_0 at which the upper eigenvalue crosses E.

EDM experiments may constrain $\Delta\varphi$ in some models [44], but it has recently been noted [41] that in other models φ_B is constrained to be small while φ_A is essentially unconstrained. Any constraints on the CP violating phases are weakened if the first and second generation squarks are heavy. Finally, note that φ_A can be generation-dependent. Hence, there is no model-independent constraint on $\Delta\varphi$ for third generation squarks.

As a concrete example which will serve as a visual aid for much of our subsequent discussion, in Figure 4.1, we plot the eigenvalues of M^2 as a function of x for the parameter set $\tilde{m}_{tL} = 110$ GeV, $\tilde{m}_{tR} = 90$ GeV, $A = \mu = 100$ GeV, $\tan\bar{\beta} = 2$, $\tan(\bar{\beta} - \Delta\beta) = 1$, that is $\Delta\beta = 0.32$, $\Delta\varphi = \pi/2$, $m_Z = 91$ GeV, $m_t = 175$ GeV, and $\sin^2\theta_W = 0.23$. With these parameters, the zero temperature masses of the two top squarks are 141 GeV and 243 GeV. In our example, we take the wall width to be $w = (4\text{ GeV})^{-1}$. Although the critical temperature T_c and the wall velocity v_w

play no role in the calculation of ΔR, we mention for completeness that when they enter in the next section, we will use $T_c = 100$ GeV and $v_w = 0.1$ as representative values. It is conventional to write the wall width in terms of the temperature, that is, $w = 25/T_c$ in our example. Henceforth, we write T_c as T when it causes no ambiguity. The final relevant parameter is the ϕ mean free path l, which will appear in Section 4.4 where we estimate $l \sim 10/T \sim 0.4w$. This completes the enumeration of the parameters specifying the "canonical" example for which we will quote results in the following. We will, of course, describe the effects of varying each of these parameters at appropriate points in the discussion.

We wish to follow a ϕ particle from the thermal ensemble in the symmetric phase that last scattered somewhere away from the wall and is now incident upon the wall. Implicit in this scenario is the assumption that the mean free path of the scalars in the plasma is long compared to the wall width w. This assumption is likely false, but we nevertheless use it in this section and the next, deferring our treatment of the suppression due to finite mean free paths for the ϕ particles to Section 4.4. The particle impinges upon the wall and is reflected or transmitted, and then resumes its thermal motion in the plasma on one side of the wall or the other. During the time between the last scattering before reflection or transmission and the first after, the particle propagates freely, experiencing only the changing expectation values of the Higgs fields which are encoded in the mass matrix. We calculate the reflection coefficients and their asymmetry in the rest frame of the wall; we will boost the resulting baryon number flux to the plasma frame when we calculate it in Section 4.3. In the wall frame, energy is conserved upon traversing the wall since the mass matrix is time-independent. The reflection coefficients can be calculated by solving the time independent Klein-Gordon equations

$$\left[\delta_{ij}(\nabla^2 + E^2) - M_{ij}^2(\mathbf{x})\right] \phi_j(\mathbf{x}) = 0 \tag{4.6}$$

because the time dependence of solutions is simply an overall $\exp(iEt)$. In general, we will take a basis in ϕ_1 and ϕ_2 such that far from the wall in the symmetric phase,

M^2 is diagonal. This has already been accomplished, since $\tilde{m}_{iL}^2$ and $\tilde{m}_{iR}^2$ are the only terms in the mass matrix (4.1) which are nonzero in the symmetric phase. When calculating the baryon number flux in Section 4.3, we will consider particles incident upon the wall with momenta that are not perpendicular to the wall. However, their reflection coefficients will depend only upon the component of their momentum that is perpendicular to the wall; so it suffices to compute reflection coefficients for normal incidence. Therefore, the problem of finding reflection coefficients is effectively a one-dimensional scattering problem, and equations (4.6) become ordinary differential equations for $\phi_j(x)$.

Consider the mass matrix whose eigenvalues are shown in Figure 4.1. The behavior of the reflection coefficients is qualitatively different for particles incident from the symmetric phase with energies $E < \mu_{s2}$, $\mu_{s2} < E < \mu_{b2}$, and $E > \mu_{b2}$. For $E < \mu_{s2}$, there is only one propagating mode in both the symmetric and the broken phases. In general, we denote the reflection coefficient for a ϕ_i incident upon the wall from the symmetric phase and reflected back into the symmetric phase as a ϕ_j by R_{ij} for particles, and denote the corresponding quantity for antiparticles by $R_{\overline{ij}}$. For $E < \mu_{s2}$, however, the only reflection coefficients are R_{11} and $R_{\overline{11}}$. Since the CPT conjugate of the reflection of ϕ_1 to ϕ_1 is the reflection of $\bar{\phi}_1$ to $\bar{\phi}_1$, we see that $R_{11} = R_{\overline{11}}$ and there is no reflection asymmetry. Before proceeding to higher energies, note that for a different mass matrix it may be the case that $\mu_{b1} > \mu_{s2}$. In this case, for $E < \mu_{b1}$ there are two propagating modes in the symmetric phase and none in the broken phase, so both ϕ_1 and ϕ_2 must be totally reflected. We now argue that in this circumstance, the reflection coefficients again cannot be CP violating. Unitarity implies that for total reflection,

$$R_{11} + R_{12} = 1 \tag{4.7}$$

$$R_{\overline{11}} + R_{\overline{12}} = 1 \tag{4.8}$$

We see that unitarity, together with $R_{11} = R_{\overline{11}}$, implies that $R_{12} = R_{\overline{12}}$, and hence there is no reflection asymmetry. For the rest of this chapter, it is implicit that

references to μ_{s2} should be replaced by references to μ_{b1} if the mass matrix is such that $\mu_{b1} > \mu_{s2}$. We have shown that particles incident from the symmetric phase with energy $E < \mu_{s2}$ yield no reflection asymmetry.

Now consider incident energies $\mu_{s2} < E < \mu_{b2}$, for which there are two propagating modes in the symmetric phase and only one in the broken phase. As shown in Figure 4.1, for any energy in this shaded range there is a point x_0 at which the larger eigenvalue of M^2 equals E^2. This means that there is a particular linear combination of incident ϕ_1 and ϕ_2 that evolves by mixing as it propagates through the wall in just such a way that upon arrival at x_0 it is purely in the mass eigenstate with eigenvalue E^2, and is therefore totally reflected. Since one linear combination of ϕ_1 and ϕ_2 is totally reflected by the wall, both R_{12} and R_{21} are large in this energy range, given sufficient mixing. In order to obtain large asymmetries between the reflection coefficients for particles and for antiparticles, the individual reflection coefficients must of course be large, making this zone of enhanced reflection a promising place to look for large ΔR. Without CP violation, the same linear combination of incident $\bar{\phi}_1$ and incident $\bar{\phi}_2$ mixes to become the mode with eigenvalue E^2 at x_0, and is totally reflected. This implies that $R_{\overline{12}} = R_{12}$ and $R_{\overline{21}} = R_{21}$. However, if the off-diagonal term in M^2 has a spatially varying phase, then the linear combination of $\bar{\phi}$'s that is totally reflected is different from that for the ϕ's, and we expect $\Delta R \neq 0$, as we confirm explicitly below.

Before proceeding, note that $R_{\overline{12}} = R_{21}$ by CPT and therefore

$$\Delta R \equiv R_{12} - R_{\overline{12}} = R_{12} - R_{21} \ . \tag{4.9}$$

This simplifies calculations by giving the reflection asymmetry in terms of reflection coefficients for particles only. Another simplification is that in the enhanced reflection zone, ΔR is the only possible asymmetry because there is no asymmetry due to particles incident from the broken phase. Denoting the single propagating mode in the broken phase by ϕ_3, since $R_{33} = R_{\overline{33}}$ by CPT, unitarity requires that incident ϕ_3's cannot yield baryon number asymmetric transmission into the symmetric phase. We

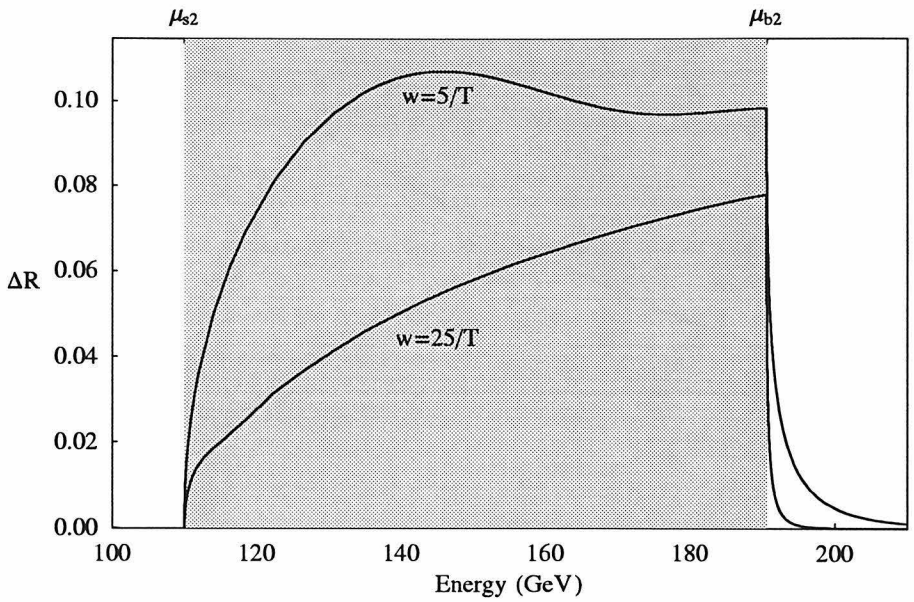

Figure 4.2: ΔR as a function of incident energy E, for two different wall widths w. The enhanced reflection zone is shaded.

give a careful explanation of the calculation of ΔR in the supplementary Section 4.6; henceforth in this section, we focus solely on the results.

In Figure 4.2, we plot ΔR vs. incident energy E for two values of the wall width, $w = 5/T$ and $w = 25/T$, with all other parameters as in our canonical example. The enhanced reflection zone is apparent, with $\Delta R \sim 0.1$ for $w = 5/T$. Even greater values of ΔR are obtained for $\Delta\beta$ and $\Delta\varphi$ that are larger than our canonical values. (For example, for $\Delta\beta = 1$ and $\Delta\varphi = 2.5$, we find $\Delta R \sim 0.3$.) We have therefore confirmed that in the enhanced reflection zone, large reflection coefficients yield large reflection asymmetries in the presence of $\mathcal{O}(1)$ CP violating phases. For incident energies below the enhanced reflection zone, $\Delta R \equiv 0$. At higher energies, that is for $E > \mu_{b2}$, there are two propagating modes in both the symmetric and the broken phases and throughout the wall. In this regime, $\Delta R \neq 0$, but it is extremely small. For $w = 5/T$, $\Delta R = 0.0047$ at $E = 200$ GeV; $\Delta R = 2.5 \times 10^{-5}$ at $E = 250$ GeV; and $\Delta R = 1.3 \times 10^{-6}$ at $E = 300$ GeV. For these energies, transmission coefficients are very close to 1 and reflection coefficients (and therefore ΔR) are very small, due to

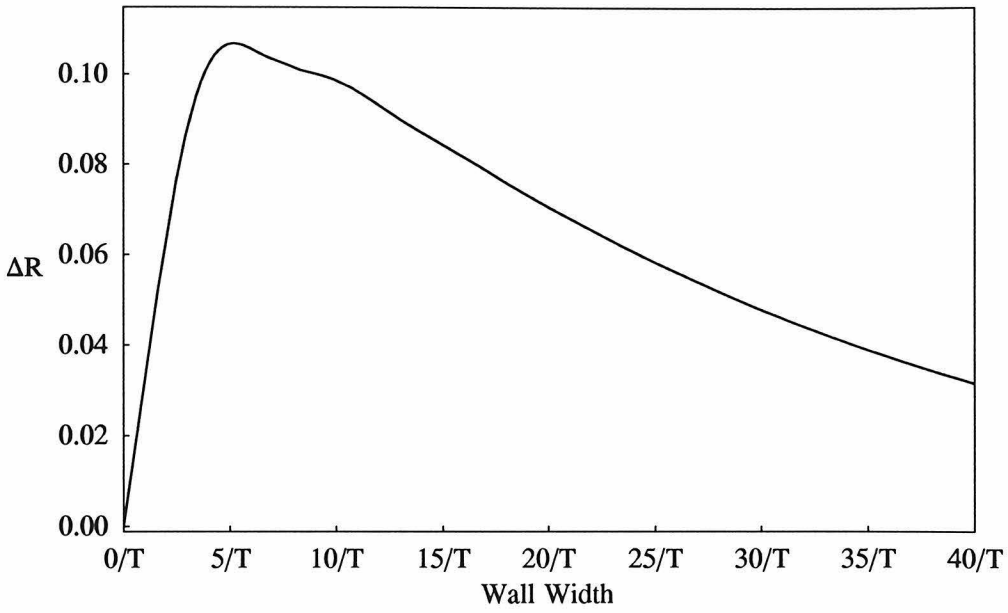

Figure 4.3: ΔR as a function of wall width w for incident energy $E = 150$ GeV, which is within the enhanced reflection zone.

the lack of total reflection.

For energies above μ_{b2}, unlike for those in the enhanced reflection zone, there is the possibility of a nonzero asymmetry arising from particles and antiparticles incident from the broken phase and transmitted through the wall into the symmetric phase. This asymmetry is very small, as we now argue. Just as the R_{ij} are very small in this energy range, the reflection coefficients for reflection of particles incident from the broken phase back into the broken phase are very small also. Since any asymmetry associated with transmission into the symmetric phase must be balanced by an asymmetry in reflection, we conclude that even though the transmission coefficients are ~ 1, their asymmetry is very small.

We now discuss the dependence of ΔR on the parameters in the problem, beginning with the wall width w. Note that in order to obtain a nonzero ΔR, there must be some region in x in which modes incident from the symmetric phase can mix, and hence feel the effects of the CP violating terms, before arriving at x_0 where one mode is totally reflected. This implies that $\Delta R = 0$ for an infinitesimally thin (step

function) wall. In the thin wall limit, R_{12} and $R_{\overline{12}}$ are large in the enhanced reflection zone, but they are equal. In Figure 4.3, we plot ΔR at $E = 150$ GeV versus the wall width w for our canonical M^2. We see that $\Delta R \sim w$ for w small relative to the inverse mass scales in the problem. At large w, the number of wavelengths per wall width grows and therefore R_{12} and $R_{\overline{12}}$ decrease, and so does ΔR. The asymmetry ΔR peaks at about $w = 5/T$, one of the values we have chosen to plot in Figure 4.2. This is an unphysically thin wall — estimates for w range from $10/T$ to $100/T$. (The physics determining w is presented, for example, in Refs. [9, 13].) In our canonical example we follow Ref. [26] and use $w = 25/T$, and we have plotted ΔR for this wall width in Figure 4.2. If w is in fact smaller than $25/T$, our final result for the BAU is enhanced, while for thicker walls, it is somewhat suppressed.

Let us now consider the effects of varying the mass parameters in M^2. We define m and Δm by

$$\begin{aligned} \mu_{s1} = \tilde{m}_{tR} &= m - \frac{\Delta m}{2} \\ \mu_{s2} = \tilde{m}_{tL} &= m + \frac{\Delta m}{2} \, . \end{aligned} \tag{4.10}$$

For simplicity, we will always take $\mu = A$ and $\tan\bar{\beta} = 2$. (The optimal choice for $\bar{\beta}$ should be such that $A \sim \mu \cot\bar{\beta}$. We find, however, that for $A = \mu$, varying $\bar{\beta}$ from 0.5 to 4 changes our results by at most 10%, so the dependence on $\bar{\beta}$ is not significant.) We have investigated the dependence of our results on m, Δm and A. Of course, we do not vary the m_Z^2 and m_t^2 terms in M^2, and these should be thought of as setting the energy scale. Varying m between 50 and 150 GeV while holding $\Delta m/m$ and A fixed changes ΔR by less than 20%. Increasing m further leads to a suppression of ΔR because it increases all the eigenvalues relative to $1/w$. For $A = 0$, there is no mixing between ϕ_1 and ϕ_2, and $\Delta R = 0$. Increasing A from 0 to 200 GeV holding all else fixed yields a monotonically increasing ΔR, but in going from $A = 100$ GeV to $A = 200$ GeV, the increase in ΔR is less than 10%. Of the three mass parameters we have varied, Δm has the biggest effect. ΔR is maximized for $\Delta m = 0$. However, we will see in the next section that the baryon number flux is identically zero for

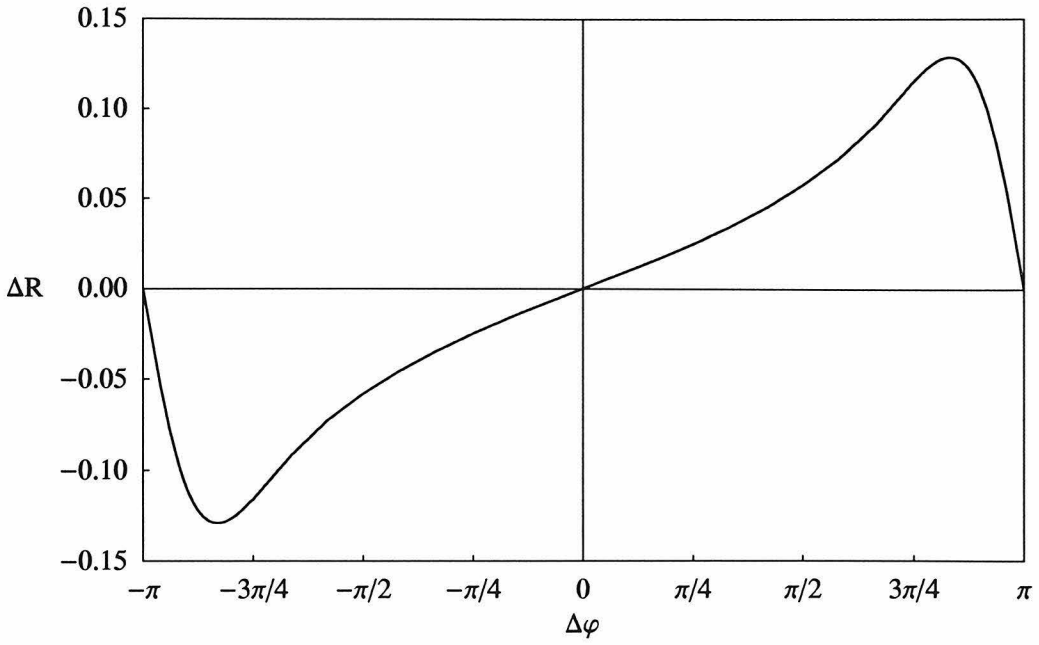

Figure 4.4: ΔR as a function of $\Delta\varphi$ for incident energy at the center of the enhanced reflection zone.

$\Delta m = 0$. As Δm is increased, ΔR falls; by a few percent at $\Delta m/m = 0.2$; by about a factor of two at $\Delta m/m = 0.8$. We defer a plot displaying the dependence of our results on Δm to the next section.

Finally, we come to the CP violating phase. We have verified that for small $\Delta\varphi$ and $\Delta\beta$, ΔR is linear in both quantities. As we have noted, there is no model-independent constraint on $\Delta\varphi$; therefore, in Figure 4.4 we show ΔR over the entire range of $\Delta\varphi$. We see that ΔR is approximately linear in $\Delta\varphi$ for $|\Delta\varphi| \leq 2$. We find that ΔR is linear in $\Delta\beta$ over the range $-0.2 < \Delta\beta < 0.5$. The values we have been using in our canonical example — $\Delta\varphi = \pi/2$ and $\Delta\beta = 0.32$ — are within the linear regime. For convenience, in subsequent sections, we often quote results assuming that $\Delta\beta$ and $\Delta\varphi$ are in their linear regimes, as is likely the case for $\Delta\beta$, but not necessarily for $\Delta\varphi$. Fortified by our understanding of how ΔR in the enhanced reflection zone varies with wall width, masses, and phases, we are ready for the next step in our computation of the BAU.

4.3 From Asymmetric Reflection Coefficients to Baryon Number Flux

We now compute the baryon number flux into the symmetric phase by integrating ΔR against the flux densities of the incident particles. The flux, which we denote by $\mathcal{F}_B$, receives two contributions. One contribution, $F_{s\to s}$, is generated by the asymmetry in the reflection of particles and antiparticles incident on the wall from the symmetric phase and is associated with ΔR. The other contribution, $F_{b\to s}$, is caused by the asymmetry in the transmission of the particles and their antiparticles incident on the wall from the broken phase. We have seen, however, that this asymmetry (unlike ΔR) is zero for energies in the enhanced reflection zone, and is small (like ΔR) at higher energies. We therefore neglect $F_{b\to s}$ and obtain

$$\mathcal{F}_B \simeq \frac{1}{3} F_{s\to s} \ . \tag{4.11}$$

The factor of $1/3$ arises because the ϕ particles have baryon number $1/3$.

Before deriving an expression for $F_{s\to s}$, we make some general observations. The processes we are studying are invariant under time translations (although not under time reversal!). Therefore, energy is conserved upon reflection from or transmission through the wall. We denote the components of a particle's momentum in the rest frame of the wall that are perpendicular and parallel to the wall by $p_{i\perp}$ and $\vec{p}_{i||}$, respectively. Recalling that M^2 is diagonal in the symmetric phase, we have

$$E^2 = p_{1\perp}^2 + p_{1||}^2 + \mu_{s1}^2 = p_{2\perp}^2 + p_{2||}^2 + \mu_{s2}^2 \ , \tag{4.12}$$

where $p_{i||} = |\vec{p}_{i||}|$. Since the processes of reflection from and transmission through the wall are invariant under spatial translations along the surface of the wall, $\vec{p}_{i||}$ is conserved. For example, for a ϕ_1 reflecting into a ϕ_2, $\vec{p}_{1||} = \vec{p}_{2||}$. Equation (4.12) then yields

$$p_{1\perp}^2 + \mu_{s1}^2 = p_{2\perp}^2 + \mu_{s2}^2 \equiv \varepsilon_\perp^2 \ , \tag{4.13}$$

defining a conserved quantity $\varepsilon_\perp$. We now see how to translate results obtained in the $(1+1)$-dimensional treatment of the previous section into the full $(3+1)$-dimensional setting appropriate here. What was called E in previous sections is in fact $\varepsilon_\perp$. ΔR depends on $\varepsilon_\perp$, and the enhanced reflection zone is given by $\mu_{s2} < \varepsilon_\perp < \mu_{b2}$.

Before the arrival of the wall, the ϕ's are in thermal equilibrium with momenta distributed according to the Bose-Einstein distribution. This equilibrium distribution defines a rest frame, the plasma frame, which is different from the rest frame of the wall. In order to compute $\mathcal{F}_B$, we need the flux density of ϕ_i particles (equivalently, $\bar{\phi}_i$ antiparticles) incident upon the wall with a given momentum in the wall frame. Throughout this section, we continue to assume that the mean free path of particles is larger than the wall width, deferring the discussion of the effects of the falseness of this assumption to Section 4.4. Hence, the incident flux density we require is given simply by

$$f_i(E, p_{i\perp}) = \frac{3p_{i\perp}/E}{e^{\gamma(E - v_w p_{i\perp})/T} - 1}, \tag{4.14}$$

where $\gamma \equiv 1/\sqrt{1 - v_w^2}$. The factor of 3 appears because there are ϕ's with each of 3 different colors in thermal equilibrium. The argument of the exponential arises because, as mentioned before, the particles are initially in thermal equilibrium in the plasma frame, not in the wall frame. To get $F_{s\to s}$, we must integrate $\Delta R \equiv R_{12} - R_{\overline{12}} = R_{12} - R_{21}$ against f_1 over the three-momentum of the incident ϕ_1 and integrate $R_{21} - R_{\overline{21}} = R_{21} - R_{12} = -\Delta R$ against f_2 over the three-momentum of the incident ϕ_2 and add up the results. Thus, we obtain

$$\begin{aligned} F_{s\to s} &= \frac{1}{\gamma}\left[\int_0^{2\pi}\int_0^{\infty} \frac{d\theta\, dp_{1\|}\, p_{1\|}}{(2\pi)^2} \int_{p_{1\perp\min}}^{\infty} \frac{dp_{1\perp}}{2\pi}\, \Delta R(p_{1\perp})\, f_1(E, p_{1\perp})\right] \\ &- \frac{1}{\gamma}\left[\int_0^{2\pi}\int_0^{\infty} \frac{d\theta\, dp_{2\|}\, p_{2\|}}{(2\pi)^2} \int_{p_{2\perp\min}}^{\infty} \frac{dp_{2\perp}}{2\pi}\, \Delta R(p_{2\perp})\, f_2(E, p_{2\perp})\right], \end{aligned} \tag{4.15}$$

where $p_{i\perp\min}$ is the value of $p_{i\perp}$ such that $\varepsilon_\perp = \mu_{s2}$. Note that $F_{s\to s}$ is the flux seen in the plasma frame. Transforming from the wall frame back to the plasma frame yields the overall factor of $1/\gamma$ in (4.15). Upon performing the integration over $p_{i\|}$,

we obtain

$$\mathcal{F}_B \simeq \frac{1}{3} F_{s\to s} = \frac{T}{4\pi^2\,\gamma^2} \int_{\mu_{s2}}^{\infty} d\varepsilon_\perp \; \varepsilon_\perp \, \Delta R(\varepsilon_\perp) \ln \left[\frac{1 - e^{-\gamma(\varepsilon_\perp - v_w p_{2\perp})/T}}{1 - e^{-\gamma(\varepsilon_\perp - v_w p_{1\perp})/T}} \right], \qquad (4.16)$$

where we have used (4.13) in the form $\varepsilon_\perp d\varepsilon_\perp = p_{1\perp} dp_{1\perp} = p_{2\perp} dp_{2\perp}$.

From (4.16), we deduce that $F_{s\to s} = 0$ for $v_w = 0$. This is to be expected, since baryogenesis requires out of equilibrium conditions, and hence requires $v_w \neq 0$. (Note that one can derive an expression for $F_{b\to s}$ similar to that for $F_{s\to s}$ and show that $F_{b\to s} = 0$ when $v_w = 0$.) The vanishing of $\mathcal{F}_B$ with v_w can be more directly understood as follows. We present the argument in $1+1$ dimensions; the generalization to $3+1$ is trivial. We have shown that $R_{12} - R_{\overline{12}} = -(R_{21} - R_{\overline{21}})$. For $v_w = 0$, the number of ϕ_1 particles incident upon the wall with an energy E greater than μ_{s2} is equal to the number of incident ϕ_2 particles with the same energy. (There are of course ϕ_1 particles with $\mu_{s1} < E < \mu_{s2}$, but they do not yield a reflection asymmetry.) Therefore, for $v_w = 0$, the contribution to $\mathcal{F}_B$ due to incident ϕ_1's is exactly cancelled by that due to incident ϕ_2's. Now consider a moving wall, so $v_w \neq 0$. ϕ_i particles incident upon the wall with a given energy E in the wall frame have energy $(E - v_w p_{i\perp})$ in the plasma frame, in which they are initially in a thermal equilibrium distribution. If $\mu_{s1} \neq \mu_{s2}$ then $p_{1\perp} \neq p_{2\perp}$ for a given E, and the number of ϕ_1 and ϕ_2 particles with incident energy E in the wall frame is *not* the same. We see that in order to upset the cancellation between the contribution to $\mathcal{F}_B$ due to incident ϕ_1's and that due to ϕ_2's, we need both $v_w \neq 0$ and $\mu_{s1} \neq \mu_{s2}$. The asymmetry in the reflection coefficients can only yield an asymmetry in the baryon number flux if the wall is moving and if the scalars are not degenerate in mass in the symmetric phase.

As discussed in the previous section, ΔR depends on parameters in M^2 and on the wall width. The flux $\mathcal{F}_B$ depends on these parameters as well as on the wall velocity and temperature. We will be interested in the regime in which v_w and $\Delta m/m$ are small compared to 1. This may seem surprising, given that we have just argued that $\mathcal{F}_B$ is zero for $v_w \to 0$ or $\Delta m/m \to 0$. The reason is that, as we have seen in the previous section, ΔR is a decreasing function of Δm and, as we will see in the next

section, the BAU is proportional to $\mathcal{F}_B/v_w^3$ for realistic wall velocities. In order to gain intuition about (4.16) it is useful to pretend that ΔR is energy independent for $\mu_{s2} < \varepsilon_\perp < \mu_{b2}$, and then expand in v_w and $\Delta m/m$ to first order in both, obtaining

$$\frac{\mathcal{F}_B}{T^3} \sim \frac{1}{4\pi^2}\, v_w\, \frac{\Delta m}{m}\, \left(\frac{m}{T}\right)^2\, \Delta R \int_{m/T}^{\mu_{b2}/T} \frac{y\, dy}{[e^y - 1]\sqrt{y^2 - (m/T)^2}} \ . \tag{4.17}$$

We perform all our calculations using (4.16), not the expansion (4.17), but the expansion is useful for understanding the qualitative dependence of $\mathcal{F}_B$ on the parameters.

With all parameters as in our canonical example, (4.16) yields

$$\frac{\mathcal{F}_B}{T^3} \sim 9 \times 10^{-6} \ , \tag{4.18}$$

and with $w = 5/T$ instead of $25/T$, we obtain a result which is a factor of two larger. We have verified that $\mathcal{F}_B$ is linear in v_w to within a few percent for $v_w < 0.6$. In the regime in which $\mathcal{F}_B$ is linear in $\Delta\beta$, $\Delta\varphi$, and v_w, (4.18) becomes

$$\frac{\mathcal{F}_B}{T^3} \sim 2 \times 10^{-4}\, v_w\, \Delta\beta\, \Delta\varphi \ . \tag{4.19}$$

Turning now to the temperature dependence, in Figure 4.5, we plot $\mathcal{F}_B/T^3$ versus m/T, varying T and keeping all parameters in the mass matrix fixed. Since ΔR does not depend on T, we can partially understand this plot by noting that in (4.17) $\mathcal{F}_B/T^3 \sim (m/T)^2$ at small m/T and $\sim \exp(-m/T)$ at large m/T. This does not completely describe the figure, however, because as we vary T, we have kept $w = 25/T$; this means that w changes with respect to the parameters in the mass matrix. We conclude from Figure 4.5 that the BAU generated by the scalar baryon number transport mechanism is largest for $m \sim T$.

In Figure 4.6, we plot $\mathcal{F}_B/T^3$ vs. $\Delta m/m$. It is linear in $\Delta m/m$ for small $\Delta m/m$ and falls at large $\Delta m/m$ because, as we noted in the previous section, ΔR decreases with increasing $\Delta m/m$. We see that using $\Delta m/m = 0.2$ as in our canonical example

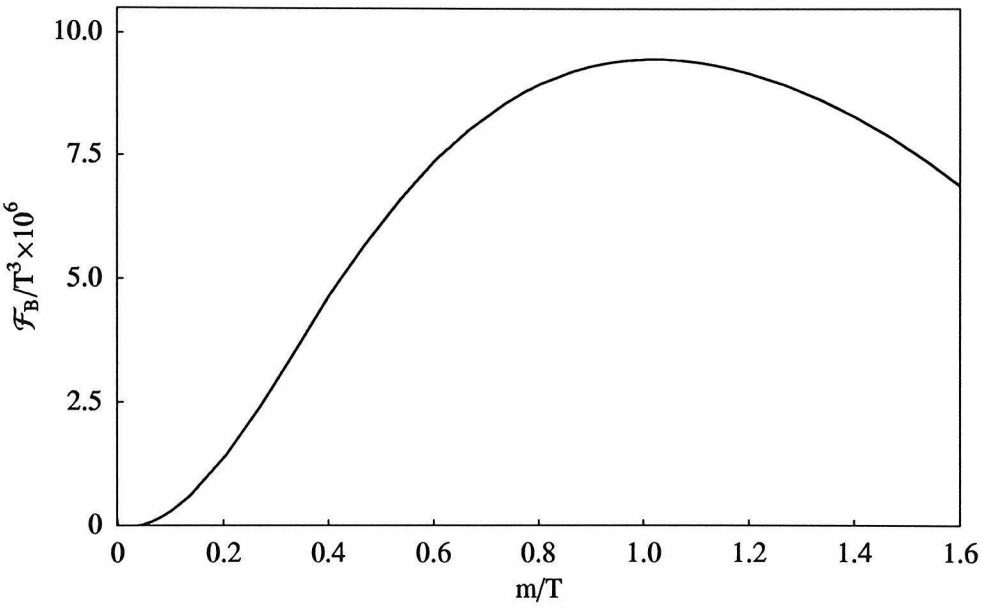

Figure 4.5: Temperature dependence of the baryon number flux. In this plot, T varies and $w = 25/T$ for all T. We keep all parameters except T and w fixed. We plot $\mathcal{F}_B/T^3$ vs. m/T to facilitate comparison with (4.17).

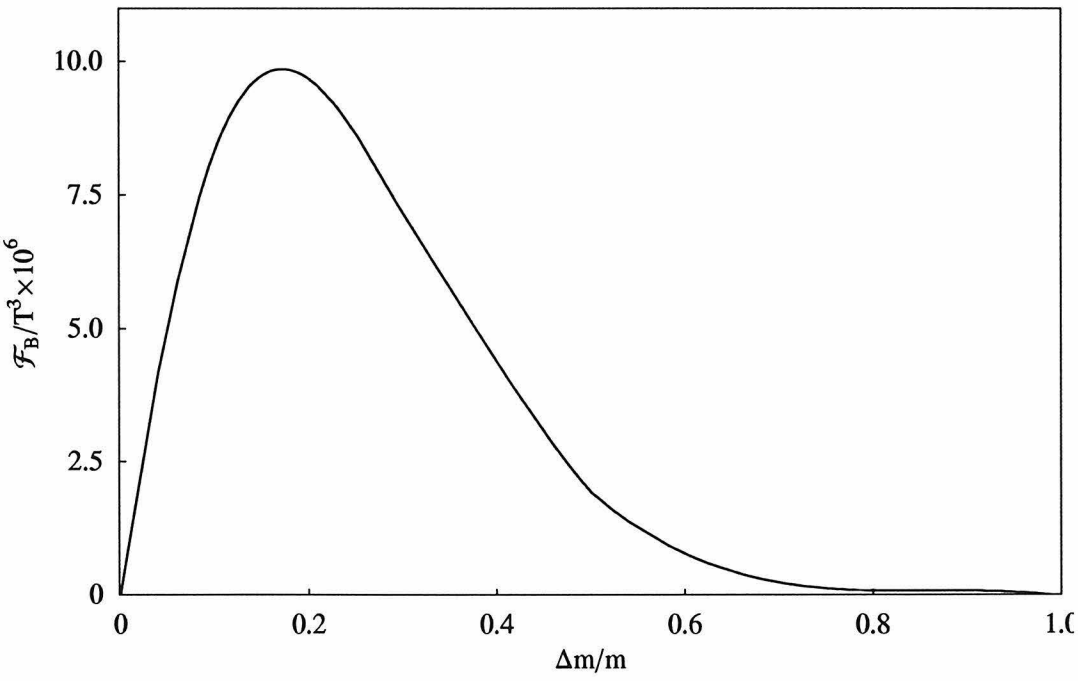

Figure 4.6: Dependence of the baryon number flux on $\Delta m/m$, with Δm varying and all other parameters fixed.

yields a reasonable estimate for ΔR over the range $0.1 < \Delta m/m < 0.3$, but for $\Delta m/m$ outside this range, the BAU is suppressed. For the scalar baryon transport mechanism to be efficient, we need scalars with symmetric phase masses of $\mathcal{O}(T_c)$ that differ by 10-30%.

4.4 Estimating the Baryon Number of the Universe

In the preceding sections, we have shown how to calculate the baryon number flux $\mathcal{F}_B$ carried by ϕ particles that is injected into the symmetric phase by the motion of the bubble wall. To this point, we have described the quantitative solution of a well-posed problem. Given a mass matrix, a critical temperature, a wall profile, a wall velocity, and making the assumption that the ϕ mean free path is long compared to the wall width, a quantitative calculation of $\mathcal{F}_B$ is attainable. In this section, we sketch a qualitative estimate of the cosmological baryon to entropy ratio, n_B/s, that results from the flux $\mathcal{F}_B$. Our treatment is admittedly crude and can be improved, for example along the lines of that of Huet and Nelson [25], but we leave this for future work. We organize the estimate of the final result as follows. First, we estimate the mean free path l and the suppression of $\mathcal{F}_B$ that results from the finiteness of l/w. Then, we estimate the scalar baryon number density (baryon number in the form of ϕ's) that results from $\mathcal{F}_B$. This in turn leads to a quark baryon number density which biases the electroweak sphaleron processes acting in the symmetric phase, resulting in a net baryon asymmetry of the universe.

Before the wall arrives, the ϕ's in the symmetric phase are meandering about in the plasma with a mean free path which we call λ and a mean velocity between scatterings which we call $\bar{v}$. The diffusion constant is defined as

$$D = \frac{1}{3}\lambda\,\bar{v}\ . \tag{4.20}$$

The mean velocity is $\bar{v} \sim 0.9$ for particles with $m = T$. In the next chapter (see

also [45]), I estimate (based upon a collaboration with Hooman Davoudiasl) that, in the symmetric phase, the diffusion constant for squarks is $D \approx 5/T$ and $\lambda \approx 18/T$, although these numbers are only reliable up to about a factor of 2. The mean velocity in one direction is then $v_\phi = \bar{v}/\sqrt{3} \approx 0.5$ and the mean free path along one direction (for instance, across the wall) is

$$l = \lambda/\sqrt{3} \approx \frac{10}{T} \ . \tag{4.21}$$

We now give a crude estimate of the suppression due to the finiteness of l/w. As noted in Section 4.2, estimates for w range from $10/T$ to $100/T$. In our canonical example, we use $w = 25/T$, yielding $l/w \sim 0.4$. The essence of the effect is that when ϕ particles reach x_0, the point in the wall at which one mode is totally reflected, they have only been travelling (and mixing) freely for a distance of order l. To incorporate this, we redo the calculation of ΔR as follows. For each incident energy, we find x_0 and choose as incident states the mass eigenstates a distance l to the left of x_0. These then propagate only a distance l before reflecting, and so experience less CP violating mixing than in the case where l is infinite. The result is a suppression in ΔR at each energy. We in fact find that this suppression is rather energy dependent, being larger for energies close to μ_{b2}. In evaluating $\mathcal{F}_B$, therefore, we must re-evaluate the integral (4.16). The result is shown in Figure 4.7, in which we plot $\mathcal{F}_B/T^3$ vs. l/w. We see that for $l/w = 0.4$, the flux $\mathcal{F}_B$ is suppressed by about a factor of 2 relative to that for infinite l. We have also verified that the reflection asymmetries at a given energy are largely insensitive to the form of the potential beyond the corresponding x_0. Although our method of including the effects of a finite mean free path is certainly not the final word, it should give a reasonable estimate of the magnitude of the suppression. Note in particular that the integrand in (4.16) is largest for lower energies within the enhanced reflection zone. For these energies, x_0 is on the symmetric phase side of the wall, and the dependence on l/w is not severe. This qualitative explanation is consistent with our result that $\mathcal{F}_B$ is only suppressed by a factor of 2 for $l/w = 0.4$.

If w is larger than $25/T$, the final result will be suppressed both by the change

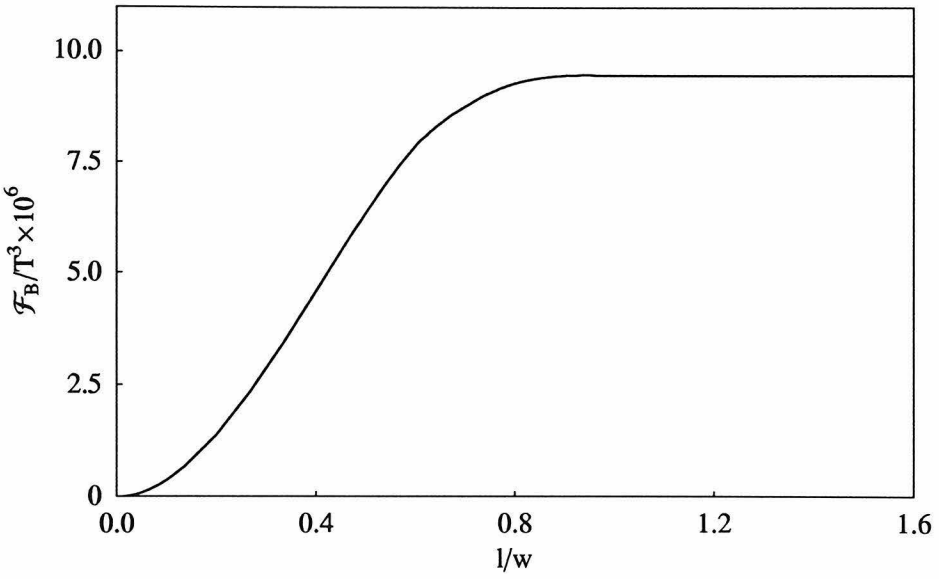

Figure 4.7: Dependence of the baryon number flux on l/w, with l varying and all other parameters fixed.

in $m\,w$ displayed in Figure 4.3 and by the effect of l/w displayed in Figure 4.7. Of course, $w < 25/T$ would correspondingly enhance the final result, for example by a factor of 4 for $w = l = 10/T$. In the estimates that follow, we take $\mathcal{F}_B/T^3 \sim 5\times10^{-6}$, as appropriate for $m = A = \mu = T = 100$ GeV, $\Delta m/m = 0.2$, $w = 25/T$, $l/w = 0.4$, $v_w = 0.1$ and $\Delta\beta\Delta\varphi = 0.5$. In the regime in which $\mathcal{F}_B$ is linear in v_w, $\Delta\beta$, and $\Delta\varphi$, we can write it as

$$\frac{\mathcal{F}_B}{T^3} \sim 1\times10^{-4}\, v_w\, \Delta\beta\, \Delta\varphi\ . \tag{4.22}$$

The dependence on the other parameters is more complicated, as we have discussed and illustrated above.

Next, we give an estimate of the baryon number density carried by ϕ particles in the region in front of the bubble wall. A ϕ particle emerging into the symmetric phase from the wall begins to diffuse, and the mean distance such particles have travelled from the wall a time t after being reflected is $x \sim \sqrt{2lv_\phi t}$. In the same time t, the wall itself has moved a distance $v_w t$. Defining τ as the time that a reflected ϕ particle

spends in the symmetric phase before the wall overtakes it, we find that on average,

$$\tau \sim \frac{2lv_\phi}{v_w^2} \ . \tag{4.23}$$

Note that this means that on average a reflected ϕ particle undergoes

$$N_{\rm scatt} \sim \frac{\tau}{l/v_\phi} \sim 2\left(\frac{v_\phi}{v_w}\right)^2 \tag{4.24}$$

scatterings during the time τ it spends in the broken phase. Our treatment is only consistent for $N_{\rm scatt} > 1$, and our final result is largest for large $N_{\rm scatt}$.

We denote the mean separation between the diffusing particle and the oncoming wall during the time the particle is in the broken phase by Δx. This quantity will cancel in the final result. Over a range of x in front of the wall given approximately by Δx, there is a net baryon number density carried by ϕ particles given by

$$n_B^\phi \sim \mathcal{F}_B \frac{\tau}{\Delta x} \ . \tag{4.25}$$

We arrive at this estimate by noting that $\mathcal{F}_B$ is the baryon number injected into the symmetric phase per unit wall area per unit time and that at any given time, the ϕ's reflected in the previous τ are in a region of order Δx ahead of the wall. Thus, we conclude that every point in the universe experiences a baryon density in ϕ particles given by (4.25) for a time

$$t^* \sim \Delta x / v_w \tag{4.26}$$

while in the symmetric phase. By this point, it should be becoming clear that n_B/s will turn out to be largest for small wall velocities. The authors of Refs. [9, 13] find wall velocities lying in the range 0.02 to 0.4, and other authors have found velocities as high as 0.9. The mechanism we are proposing will be most effective at the lower end of this range, and we have been using $v_w \sim 0.1$ in our canonical example. Note also that we are assuming that n_B^ϕ/T^3 is small, and hence we are not including the effect of the baryon number asymmetry in the distribution functions used in the calculation

of $\mathcal{F}_B$ in the previous section.

The mechanism that generates the baryon number flux carried by ϕ particles into the symmetric phase does not involve any baryon number violation. Therefore, the baryon number associated with n_B^ϕ must be exactly cancelled by a baryon number of opposite sign behind the wall. Note that the ϕ particles, being scalars, are not produced anomalously in electroweak sphaleron processes, and therefore cannot bias such processes. Thus, if this were the end of the story, we would have made no progress. However, ϕ particles can be converted into quarks. This is a model-independent statement, equivalent to the statement that the ϕ's have baryon number 1/3. The rate for ϕ–quark conversion is, however, model dependent. In the supersymmetric case we are using as an example, if the gluino mass $M_{\tilde{g}}$ is less than μ_{s2}, the symmetric phase mass of the heavier squark, then the squarks can decay into gluinos and quarks, since the quarks are massless in the symmetric phase. We will not assume that the gluinos are this light, however. The first process we consider is scattering off a gluino in the thermal bath: squark + gluino $\rightarrow$ quark + gluon. The rate for this process is suppressed relative to that for squark-gluon scattering by $\exp(-M_{\tilde{g}}/T)$ due to the paucity of gluinos in the plasma. It is also suppressed by $(T/M_{\tilde{g}})^2$ in the cross section. The second process we consider is gluon + squark $\rightarrow$ quark + virtual gluino, where the gluino becomes quark + anti-squark or anti-quark + squark. This rate is suppressed relative to ordinary quark-gluon scattering by of order $\alpha_s(T/M_{\tilde{g}})^2$, and by three-body phase space. Defining $1/b$ as the fraction of scatterings incurred by a ϕ particle in the symmetric phase that turn the ϕ into a quark, we estimate that $b \sim 200$ for $M_{\tilde{g}} \sim 300$ GeV, noting again that this estimate is quite model dependent. We can now estimate that the baryon number density carried by quarks in the region Δx in front of the wall is

$$n_B^q \sim n_B^\phi \frac{N_{\rm scatt}}{b} \sim n_B^\phi \frac{2\,v_\phi^2}{b\,v_w^2}\ , \tag{4.27}$$

where we have used (4.24). This estimate is only valid for $N_{\rm scatt}/b < 1$; if $N_{\rm scatt}/b > 1$ then the squark–quark conversion reactions have time to establish chemical equilib-

rium, and an analysis in terms of chemical potentials should be used. For $N_{\rm scatt}/b \sim 1$, which is relevant for $M_{\tilde{g}} \sim 300$ GeV and $v_w \sim 0.1$, the average ϕ is converted to a quark at some point during its $N_{\rm scatt}$ scatterings, which leads us to estimate that the baryon number density in quarks is

$$n_B^q \sim \frac{n_B^\phi}{2} \sim \mathcal{F}_B \frac{\tau}{2\Delta x} \ , \tag{4.28}$$

where we have used (4.25). The density n_B^q *does* bias electroweak sphaleron processes. Note that a baryon number density in front of the wall cannot be affected by non-perturbative QCD processes. This is in contrast to what happens in many other mechanisms. For example, if an axial baryon number density (more left-handed quarks than right-handed ones; no net excess of baryons) is generated, this can bias electroweak sphaleron processes only if it is not first wiped out by QCD processes.

The rate per unit volume of baryon number violating sphaleron processes in the symmetric phase is conventionally written as

$$\Gamma_s \sim \kappa \alpha_W^4 T^4 \tag{4.29}$$

where $\kappa = (29 \pm 6)\alpha_W$ (see Eq. 2.1 and the discussion that follows). In thermal equilibrium, no net baryon asymmetry is generated by these processes, since sphaleron and "anti-sphaleron" processes occur at the same rate. However, in a region with a nonzero n_B^q, the sphaleron processes tend to reduce the baryon number density. In particular [46, 12]

$$\dot{n}_B \sim -6\, n_B^q \, \frac{\Gamma_s}{T^3} \ . \tag{4.30}$$

Assuming that $\Gamma_s t^*/T^3 < 1$, which is certainly the case for $v_w > 0.005$, then the net change in n_B due to anomalous electroweak processes is

$$\Delta n_B = -6\, n_B^q \, \frac{\Gamma_s}{T^3} t^* \ . \tag{4.31}$$

Long after the electroweak phase transition, after the universe has re-homogenized,

the remaining excess baryon number density will be given by Δn_B. Note that in order to end up with a baryon density in the universe today, the phase in the mass matrix M^2 must be such that $\mathcal{F}_B$ is negative. A net flux of anti-baryons is injected into the symmetric phase, compensated by a baryon flux from the wall into the broken phase. Some fraction of the anti-baryon excess in front of the wall is wiped out by sphaleron processes and after the entire universe is swept by the broken phase, a positive baryon number asymmetry persists at temperatures below T_c.

Using (4.31), (4.29), (4.28), (4.26) and (4.23), and noting that the cosmological entropy density at the time of the electroweak phase transition is $s = (2\pi^2 g^*/45)T^3 \sim 55T^3$ with g^* the number of degrees of freedom in equilibrium, we estimate that the mechanism we have presented yields a baryon to entropy ratio[3]

$$\frac{n_B}{s} \sim \frac{6}{55}\,\kappa\alpha_W^4\,\frac{l\,T\,v_\phi}{v_w^3}\,\frac{\mathcal{F}_B}{T^3}\ . \tag{4.32}$$

Inserting the expression (4.22) for the baryon number flux $\mathcal{F}_B$, valid in the regime in which $\mathcal{F}_B$ is linear in v_w, $\Delta\beta$ and $\Delta\varphi$, and using $v_\phi \sim 0.5$ and $l \sim 10/T$, we obtain

$$\frac{n_B}{s} \sim 7 \times 10^{-11}\,\frac{\kappa}{v_w^2}\,\Delta\beta\,\Delta\varphi\ . \tag{4.33}$$

As we have discussed, this result is obtained for baryon number carrying scalars with symmetric phase masses of $\mathcal{O}(T_c)$ that are non-degenerate by $\Delta m/m \sim 0.1 - 0.3$. The result (4.33) is sensitive to the wall width w. If we optimistically use $w = 10/T$ instead of $w = 25/T$, the BAU increases by a factor of 4 relative to that of (4.33).

The asymmetry (4.33) is at an interesting level. For example, if $v_w \sim 0.1$, a BAU consistent with cosmological observation is obtained for

$$\Delta\beta\Delta\varphi > 0.004, \tag{4.34}$$

where we have used $\kappa \sim 29\alpha_W \sim 1$ [19]. Taking $v_w = 0.1$ as we have done is

[3]Although our final expression has powers of v_w in the denominator, the derivation relies on (4.31), which is only valid for $\Gamma_s t^*/T^3 < 1$, and the BAU does not in fact diverge for $v_w \to 0$.

reasonable, but wall velocities as low as $v_w \sim 0.02$ are possible [9, 25]. Therefore, making the most optimistic choice for v_w, we find that the scalar baryon number transport mechanism can yield a BAU consistent with cosmological observation for $\Delta\beta\Delta\varphi > 2 \times 10^{-4}$, or even $\Delta\beta\Delta\varphi > 4 \times 10^{-5}$ if $w = 10/T$. Making more reasonable choices for w and v_w yields (4.34). We see that even if we use the conservative estimate $\Delta\beta \sim 0.01 - 0.03$ [26, 43], no strong constraints need be imposed on $\Delta\varphi$ in order for our implementation of the scalar baryon number transport mechanism using top squarks to yield a BAU consistent with cosmological observation.

We have demonstrated that the scalar baryon number transport mechanism can yield a cosmologically interesting BAU, and have done so via a supersymmetric implementation of the mechanism. It is therefore interesting to compare our result to those of other authors who have studied electroweak baryogenesis in supersymmetric theories. Most recent treatments [17, 26, 27, 28] have included one stop with a light broken phase mass, in order to have a strongly first order phase transition so that the BAU which is generated is preserved [17], but they have used symmetric phase stop masses which are much larger than T_c. In this regime, our mechanism is not effective. These treatments have used particles other than stops and have used the charge transport mechanism. Given the new results of Moore [38], they have likely underestimated the effects of strong interaction processes which wash out axial baryon number. Nevertheless, it seems likely that for masses such that the scalar baryon number transport mechanism is efficient, the contribution from charge transport involving particles other than stops is comparable to that which we find.[4]

The one treatment other than ours that includes reasonably small symmetric phase stop masses is the work of Huet and Nelson [25], and we now attempt a more quantitative comparison with their results. For one of their sets of parameters,[5]

[4]All the mechanisms we discuss in this work are "non-local," in the sense that the relevant CP violation occurs at the bubble walls, while the relevant B violation occurs away from the bubble walls in the symmetric phase. Local mechanisms, in which CP violation acts directly to bias the gauge and Higgs dynamics of sphaleron processes, have also been considered [47, 48, 49, 50] and also make a contribution to the BAU. The work of Ref. [50] suggests that for the thin wall case of interest in this work, the local contribution to the BAU is likely small.

[5]Note that a completely quantitative comparison between our results and those of Huet and Nelson is actually not possible, because they choose to neglect those diagonal terms in M^2 of (4.1)

namely $m = 150$ GeV, $A = \mu = 50$ GeV and $T_c = 60$ GeV, they find a contribution to the BAU due to stops using the charge transport mechanism given by $n_B/s \sim 2.3 \times 10^{-10} v_w(\kappa/\kappa')\Delta\beta\Delta\varphi$. Just as κ parametrizes the rate for electroweak baryon number violating processes, κ' parametrizes the rate for strong axial baryon number violating processes. The factor (κ/κ') is conventionally taken to be ~ 1, but the work of Moore [38] suggests that it is in fact smaller. For $v_w \sim 0.1$, the BAU (4.33) generated by the scalar baryon number transport mechanism is a factor of $400\kappa'$ larger than that generated by charge transport involving stops. Although the mass matrix used in Ref. [25] is not given by (4.1), it seems plausible that when the scalar baryon number transport mechanism is efficient, namely for $m \sim T$, $\Delta m/m \sim 0.1 - 0.3$, it yields the dominant stop contribution to the BAU. Huet and Nelson also consider the contribution to the BAU due to charge transport involving particles other than stops and find $n_B/s \sim 6.5 \times 10^{-9} v_w(\kappa/\kappa')\Delta\beta \sin\varphi_B$. This is somewhat smaller than (4.33), but only by a factor of $15\kappa'$ if $\varphi_B \sim \Delta\varphi$. Note, however, that in some models [41] φ_B is suppressed while $\Delta\varphi$ is not. Nevertheless, a complete treatment of the BAU should include the contribution due to charge transport involving particles other than stops. Although perhaps not the whole story, scalar baryon number transport yields the dominant contribution to the BAU due to stops, and can explain the cosmologically observed value given quite plausible model parameters.

4.5 Open Questions and Model Implementations

We have given our quantitative conclusions in the final four paragraphs of the previous section; the present section is devoted to unresolved questions and to a discussion of possible implementations of the scalar baryon number transport mechanism. We have organized our presentation of the scalar baryon number transport mechanism in such a way that all the parts of the treatment requiring technical improvement

---

proportional to m_Z^2 and m_t^2. This may be justifiable for $m = 150$ GeV, and we therefore compare our results with those they obtain using this parameter set. For their other set of parameters, which has $m = 60$ GeV, $A = \mu = 50$ GeV, their M^2 has one negative eigenvalue in the broken phase, rendering comparison to results they obtain with these parameters difficult.

were deferred to Section 4.4, in which we restricted ourselves to making estimates. For example, our treatment of the suppression due to finite mean free paths can be improved. There are many other ways to improve the arguments of Section 4.4. Moving beyond the technical, we noted at the end of Section 4.4 that a more complete treatment should include the transport of charges other than baryon number carried by the scalars of interest. Also, we have neglected thermal contributions to particle masses. Since they are of order couplings times T_c, and since the scalars we discuss have masses of order T_c in the symmetric phase and somewhat higher in the broken phase, neglecting thermal masses in this exploratory treatment of the scalar baryon number transport mechanism is justified.

The crucial observation that makes the scalar baryon number transport mechanism possible is the existence of a broad enhanced reflection zone, a range of incident energies in which reflection coefficients and their CP violating asymmetries are large. This arises when there are a different number of propagating modes at a given energy on the two sides of the wall. A broad enhanced reflection zone may arise in contexts other than that which we have considered, for example with scalars that do not carry baryon number. This suggests that insights gained from this work may have wider application.

As noted in the introduction, our main goal in this work has been to present the scalar baryon number transport mechanism, not to address model building issues. We have chosen to work within a supersymmetric scenario. Within this context, we now discuss some lessons for future model building efforts. It has already been realized [17] that it is desirable for one stop to have a zero temperature mass less than the top mass, because this assists in making the electroweak phase transition more strongly first order. We now see that it is also advantageous to have symmetric phase masses that are of order $T_c \sim 100$ GeV, and that differ by 10-30%. It will be interesting to look for supersymmetric models satisfying this criterion. As noted in Section 4.2, non-degeneracy of the appropriate magnitude arises in some models [41] due to renormalization group calculations which run down the masses from a high energy scale at which the stops are degenerate.

We have called our mechanism scalar baryon number transport rather than stop baryon number transport deliberately. The essential features of our mechanism can be implemented in other extensions of the Standard Model involving baryon number carrying scalars, although such extensions are perhaps not as well motivated as the supersymmetric scenario. The recent HERA anomaly [34] may hint at the existence of first generation scalar leptoquarks of zero temperature mass ~ 200 GeV. (See, for example, the treatment of Babu *et al.* [51].) A scalar leptoquark is a particle with a Yukawa coupling to a quark and a lepton, which therefore carries both lepton and baryon number. Suppose that there are three generations of leptoquarks diagonally coupled to the three generations of quarks and leptons by their Yukawa couplings. In a model with two Higgs doublets H_1 and H_2, couplings of the form $H_i H_j \phi_\alpha \phi_\beta$, where $i,j = 1,2$ and $\alpha,\beta = 1,2,3$, can contribute to the masses of the leptoquarks in the broken phase and provide CP violating mixing. If the leptoquark masses receive other contributions that are nonzero in the symmetric phase, then a mass matrix of the required form can arise. (In fact, if contributions beyond tree-level are included, CP violating mixing terms can arise even in a theory with a single Higgs field.) The simplest possibility, namely mixing between first and second generation leptoquarks, is tightly constrained by bounds arising from the non-observation of flavor changing neutral currents [51], and probably cannot yield large enough off-diagonal terms in the mass matrix to be of interest. However, such bounds are absent or much weaker for $\phi_2 - \phi_3$ or $\phi_1 - \phi_3$ mixing. Implementing the scalar baryon number transport mechanism using leptoquarks is therefore possible. It requires symmetric phase masses of $\mathcal{O}(T_c)$, but since the zero temperature masses receive additional contributions proportional to the Higgs vacuum expectation values, these can still be ~ 200 GeV or higher. It is possible to construct leptoquark theories that are consistent with experiment in which the scalar baryon number transport mechanism generates a BAU consistent with observation.

Let us hope nature is such that the stop (or leptoquark) spectrum is soon within reach of experiment, enabling us to discover whether the mass matrix is such that the observed cosmological baryon asymmetry can be due to scalar baryon number

transport. The mechanism is efficient if there are two scalars with symmetric phase masses of order T_c that differ by 10-30%, and if the bubble walls during the electroweak phase transition are sufficiently slow and sufficiently thin, as we have discussed in our conclusions presented in the previous section. Under such circumstances, the baryon number flux produced by reflection of scalars with incident energies in the enhanced reflection zone can easily lead to a baryon asymmetry of the universe consistent with cosmological observation.

4.6 Calculation of the Reflection Coefficients

In this section, we describe the method for numerically evaluating the reflection coefficients used in Section 4.2. We want to find solutions to the time-independent two field Klein-Gordon equation (4.6). Solutions to these second order linear ordinary differential equations are uniquely determined by specifying four boundary conditions on the fields and/or their first derivatives. Along with the linearity of the differential equations, this implies that the solutions form a linear vector space of complex dimension four.

As discussed in Section 4.2, because particles incident from the broken phase do not yield significant asymmetries, we need only consider the problem of calculating the reflection coefficients for ϕ's incident from the symmetric phase. In order to calculate R_{12}, for instance, we must find a solution that satisfies the following conditions: At large negative x in the symmetric phase, ϕ_1 has a right-moving (*i.e.*, incident) component with unit amplitude and ϕ_2 has no right-moving component. There is no restriction on the left-moving plane waves in the symmetric phase — their amplitudes determine the reflection coefficients. In the enhanced reflection zone, the solutions in the broken phase have one propagating mode, which must be purely right-moving, and one non-propagating mode, which must decay (rather than grow) exponentially for $x \to \infty$.

In the relevant solutions, the propagating modes in the broken phase must be purely right-moving (*i.e.*, outgoing), and the non-propagating modes must be expo-

nentially decaying. These two broken phase boundary conditions, one for each mode, restrict the space of relevant solutions to a two-dimensional subspace of the complete four-dimensional solution space. In the basis of interest to us, the two solutions spanning this subspace correspond to an incident symmetric phase ϕ_1 with no incident ϕ_2 and to an incident symmetric phase ϕ_2 with no incident ϕ_1. To find these basis solutions directly requires imposing boundary conditions in the symmetric phase. Imposing two boundary conditions at large positive x and two at large negative x yields a more time consuming numerical task than imposing four boundary conditions at one point. Instead, we proceed as follows. We first find two linearly independent solutions satisfying the broken phase boundary conditions, but not the symmetric phase boundary conditions. We find each solution by imposing four boundary conditions at one point in the broken phase and using the Runge-Kutta algorithm built into *Mathematica* [52]. These two solutions form a basis for the subspace of solutions satisfying the broken phase boundary conditions, and we find the basis of interest, namely the solutions satisfying the symmetric phase boundary conditions, by taking linear combinations.

The boundary conditions described above should in general be imposed at spatial infinity. We find solutions satisfying boundary conditions at finite x_+ in the broken phase and at finite x_- in the symmetric phase. Because we have chosen our profile function $p(x)$ of (4.2) such that the mass matrix does not vary for $x < -w/2$ and for $x > +w/2$, we can set $x_+ = w/2$ and $x_- = -w/2$ without loss of accuracy. For a different profile function, for instance one with exponential tails, one would have to choose x_- and x_+ far enough out on the tails to achieve the desired accuracy.

In Section 4.4, we discuss a method for obtaining a crude estimate of the effects of a finite mean free path. Instead of imposing boundary conditions at $x_- \to -\infty$ (equivalently for our profile function, $x_- = -w/2$), we impose them at $x_- = x_0 - l$. Here, x_0 is the point where one mode is totally reflected and is found by setting one of the eigenvalues of the mass-squared matrix equal to E^2 and l is the mean free path. In order to implement this calculation, in the formalism we present below we keep x_- a free parameter.

We begin by finding two solutions, solution$_\alpha$ and solution$_\beta$, by matching at x_+ to the following right-moving solutions:

$$\begin{aligned} \text{solution}_\alpha\text{:} \quad & \vec{\phi}(x) = Ae^{-ip_{b1}x}\vec{u}_{b1} \\ \text{solution}_\beta\text{:} \quad & \vec{\phi}(x) = Be^{-ip_{b2}x}\vec{u}_{b2} \end{aligned} \tag{4.35}$$

where $p_{b1} = \sqrt{E^2 - \mu_{b1}^2}$ and $p_{b2} = \sqrt{E^2 - \mu_{b2}^2}$ are the momenta of the normal modes in the broken phase at $x = x_+$; μ_{b1} and μ_{b2} are the masses of these normal modes, defined as the square roots of the eigenvalues of the mass-squared matrix in the broken phase; and $\vec{u}_{b1}$ and $\vec{u}_{b2}$, the eigenvectors of the broken phase mass-squared matrix, define the broken phase normal modes in the symmetric phase $\vec{\phi} = (\phi_1, \phi_2)$ basis. If a mode has real momentum, (4.35) ensures that it is right moving, since the time dependence of all modes is $\exp(iEt)$. If a mode is non-propagating, as one mode is in the enhanced reflection zone, its momentum should be taken to be negative imaginary to give a decaying exponential and not a growing one. Matching to the asymptotic solutions (4.35) is equivalent to imposing the boundary conditions

$$\begin{aligned} \text{solution}_\alpha\text{:} \quad & \vec{\phi}(x_+) = \vec{u}_{b1}; \quad \vec{\phi}'(x_+) = -ip_{b1}\vec{u}_{b1} \\ \text{solution}_\beta\text{:} \quad & \vec{\phi}(x_+) = \vec{u}_{b2}; \quad \vec{\phi}'(x_+) = -ip_{b2}\vec{u}_{b2} \end{aligned} \tag{4.36}$$

at $x = x_+$. Solutions to the Klein-Gordon equation (4.6) with these complete one-point boundary conditions are easily found. The solutions that satisfy the symmetric phase boundary conditions are linear combinations of solution$_\alpha$ and solution$_\beta$. Note that if w is too large, we will run into difficulty in the enhanced reflection zone. We impose boundary conditions at x_+, and find solution$_\alpha$ and solution$_\beta$ by evolving toward smaller x. These solutions include one mode that grows exponentially as x is reduced, until x reaches x_0. Therefore, if $x_+ - x_0$ is too large, the task of finding the solutions that satisfy the symmetric phase boundary conditions involves small differences between exponentially large quantities. We have found that going beyond $w = 40/T$ requires about 30-digit working precision, and is therefore prohibitive.

In order to obtain the desired linear combinations of solution$_\alpha$ and solution$_\beta$, it is necessary to know the amplitudes of the incident and reflected components of both ϕ_1 and ϕ_2 in the symmetric phase for both solution$_\alpha$ and solution$_\beta$. At the point x_- in the symmetric phase, we denote the eigenvectors of the mass-squared matrix defining the modes ϕ_1 and ϕ_2 by $\vec{u}_{s1}$ and $\vec{u}_{s2}$ (orthogonal because M^2 is Hermitian), the masses (square roots of the corresponding eigenvalues) by μ_{s1} and μ_{s2}, and the corresponding momenta by $p_{s1} = \sqrt{E^2 - \mu_{s1}^2}$ and $p_{s2} = \sqrt{E^2 - \mu_{s2}^2}$. Then the solutions at x_- will be of the form

$$\begin{aligned} \text{solution}_\alpha : \vec{\phi}(x) &= A_{\alpha 1} e^{-ip_{s1}x}\vec{u}_{s1} + B_{\alpha 1} e^{+ip_{s1}x}\vec{u}_{s1} + A_{\alpha 2} e^{-ip_{s2}x}\vec{u}_{s2} + B_{\alpha 2} e^{+ip_{s2}x}\vec{u}_{s2} \\ \text{solution}_\beta : \vec{\phi}(x) &= A_{\beta 1} e^{-ip_{s1}x}\vec{u}_{s1} + B_{\beta 1} e^{+ip_{s1}x}\vec{u}_{s1} + A_{\beta 2} e^{-ip_{s2}x}\vec{u}_{s2} + B_{\beta 2} e^{+ip_{s2}x}\vec{u}_{s2} \end{aligned} \tag{4.37}$$

where the A's and B's vary only slowly with x near x_- provided the mass matrix does not change much on length scales comparable to the wavelengths of the modes there. This condition is identically satisfied for $x_- \leq -w/2$, and is very well satisfied at larger values of x_- for a wall width $25/T$. We now write the amplitudes in (4.37) in terms of $\vec{\phi}$ and its first derivative at $x = x_-$. The amplitude $A_{\alpha j}$ of the incident component of mode j in solution$_\alpha$ is given by

$$A_{\alpha j} = e^{+ip_{sj}x_-}\vec{u}^*_{sj} \cdot \frac{(ip_{sj} - \partial_x)}{2ip_{sj}}\vec{\phi}(x_-). \tag{4.38}$$

The amplitude $B_{\alpha j}$ of the reflected component of mode j in solution$_\alpha$ is given by

$$B_{\alpha j} = e^{-ip_{sj}x_-}\vec{u}^*_{sj} \cdot \frac{(ip_{sj} + \partial_x)}{2ip_{sj}}\vec{\phi}(x_-). \tag{4.39}$$

The expressions for solution$_\beta$ are analogous.

The solutions that have incident modes in the symmetric phase that are either purely ϕ_1 or purely ϕ_2 can now be constructed from the amplitudes $A_{\alpha j}$, $A_{\beta j}$, $B_{\alpha j}$ and $B_{\beta j}$. The solution with incident ϕ_1 and no incident ϕ_2 is the linear combination

of solution$_\alpha$ and solution$_\beta$ for which the A_2 terms cancel, namely

$$\text{solution}_1\text{: } A_{\beta 2}\ \text{solution}_\alpha - A_{\alpha 2}\ \text{solution}_\beta\ . \tag{4.40}$$

Solution$_1$ can be written in the form (4.37), with coefficients

$$\begin{aligned} A_{11} &= A_{\beta 2}A_{\alpha 1} - A_{\alpha 2}A_{\beta 1} \\ A_{12} &= A_{\beta 2}A_{\alpha 2} - A_{\alpha 2}A_{\beta 2} = 0 \\ B_{11} &= A_{\beta 2}B_{\alpha 1} - A_{\alpha 2}B_{\beta 1} \\ B_{12} &= A_{\beta 2}B_{\alpha 2} - A_{\alpha 2}B_{\beta 2}\ . \end{aligned} \tag{4.41}$$

These coefficients are the amplitudes of the incident and reflected modes in solution$_1$. Similarly, the solution with incident ϕ_2 and no incident ϕ_1 is

$$\text{solution}_2\text{: } A_{\beta 1}\ \text{solution}_\alpha - A_{\alpha 1}\ \text{solution}_\beta \tag{4.42}$$

with amplitudes

$$\begin{aligned} A_{21} &= A_{\beta 1}A_{\alpha 1} - A_{\alpha 1}A_{\beta 1} = 0 \\ A_{22} &= A_{\beta 1}A_{\alpha 2} - A_{\alpha 1}A_{\beta 2} \\ B_{21} &= A_{\beta 1}B_{\alpha 1} - A_{\alpha 1}B_{\beta 1} \\ B_{22} &= A_{\beta 1}B_{\alpha 2} - A_{\alpha 1}B_{\beta 2}. \end{aligned} \tag{4.43}$$

We now have all the ingredients necessary to construct the reflection coefficients R_{ij}. (Note that as shown in Section 4.2, $R_{\overline{ij}} = R_{ji}$.)

The reflection coefficient R_{ij} is defined to be the ratio of the reflected ϕ_j current into the symmetric phase to the incident ϕ_i current from the symmetric phase. The current represented by a solution $\phi(x)$ is $i(\partial_x\phi^*)\phi - i\phi^*(\partial_x\phi)$. For a solution $Ae^{i(Et-px)}$,

this current is $2|A|^2\text{Re}\,(p)$. Hence the reflection coefficients are:

$$\begin{aligned}
R_{11} &= \left|\frac{B_{11}}{A_{11}}\right|^2 \frac{\text{Re}\ p_{s1}}{\text{Re}\ p_{s1}} = \left|\frac{A_{\beta 2}B_{\alpha 1} - A_{\alpha 2}B_{\beta 1}}{A_{\beta 2}A_{\alpha 1} - A_{\alpha 2}A_{\beta 1}}\right|^2 \\
R_{12} &= \left|\frac{B_{12}}{A_{11}}\right|^2 \frac{\text{Re}\ p_{s2}}{\text{Re}\ p_{s1}} = \left|\frac{A_{\beta 2}B_{\alpha 2} - A_{\alpha 2}B_{\beta 2}}{A_{\beta 2}A_{\alpha 1} - A_{\alpha 2}A_{\beta 1}}\right|^2 \frac{\text{Re}\ p_{s2}}{\text{Re}\ p_{s1}} \\
R_{21} &= \left|\frac{B_{21}}{A_{22}}\right|^2 \frac{\text{Re}\ p_{s1}}{\text{Re}\ p_{s2}} = \left|\frac{A_{\beta 1}B_{\alpha 1} - A_{\alpha 1}B_{\beta 1}}{A_{\beta 1}A_{\alpha 2} - A_{\alpha 1}A_{\beta 2}}\right|^2 \frac{\text{Re}\ p_{s1}}{\text{Re}\ p_{s2}} \\
R_{22} &= \left|\frac{B_{22}}{A_{22}}\right|^2 \frac{\text{Re}\ p_{s2}}{\text{Re}\ p_{s2}} = \left|\frac{A_{\beta 1}B_{\alpha 2} - A_{\alpha 1}B_{\beta 2}}{A_{\beta 1}A_{\alpha 2} - A_{\alpha 1}A_{\beta 2}}\right|^2 .
\end{aligned} \tag{4.44}$$

Chapter 5 Diffusion and Decoherence in the Electroweak Plasma

5.1 Introduction

As the previous chapter discussing the scalar baryon number transport mechanism shows, one class of parameters of the electroweak plasma that is crucial for quantitative predictions in baryogenesis is the diffusion constants of the various participating particle species. The diffusion constant and mean free path for squarks were unknown until Hooman Davoudiasl and I calculated them in Ref. [45]. We now discuss the computation of these parameters.

In Refs. [32, 53], a set of approximations in conjunction with the Boltzmann equation for quarks in the plasma of MSM particles were used to estimate the quark diffusion constant D_q. As strong interactions dominate the diffusion process, and since stops are strongly interacting particles, it has been assumed that the estimate $D_q \sim 6/T$ of Ref. [32] is applicable to stops as well (the validity of this assumption is not *a priori* obvious because of the different statistics, masses, and couplings of squarks and quarks). This estimate is derived using an approximate gluon propagator with the thermal mass of the longitudinal gluons m_g as an infrared cutoff and ignoring the different thermal properties of the transverse and longitudinal gluons. The use of the approximate gluon propagator can only yield the leading-logarithmic behavior and does not result in the correct leading α_s^2 non-logarithmic contribution [32, 53]. However, the diffusive process is expected to be dominated by the t-channel gluon exchange diagrams, and for these diagrams, the leading logarithm contribution is expected to be dominant [32]. A more comprehensive treatment in Ref. [53] gives $D_q \sim 3/T$. Again, this estimate is at the level of the leading logarithm.

To study the diffusion of particles in a plasma, one must consider scattering pro-

cesses in which the momentum transfer q is not small. For the processes we consider in this work, which are dominated by t-channel scattering, this amounts to an infrared regularization of q. This regularization is implemented naturally by the longitudinal and transverse thermal masses of the exchanged gluons, which are comparable in magnitude to the temperature T of the plasma. Since the typical momenta of the scattering particles are also of order T, this regularization provides an effective cutoff for $q \ll T$. In this chapter, we calculate the elastic[1] mean free path λ associated with these diffusive processes and relate it to the diffusion constant D. Henceforth, the words "mean free path" refer to this diffusive mean free path.

In electroweak baryogenesis scenarios that use charge transport, the CP violating interactions of the charge carriers with an expanding Higgs wall eventually result in the generation of baryon number. However, within the Higgs wall, multiple scatterings in which the final momentum of the charge carrier differs significantly from its initial momentum wash out the asymmetry caused by CP violation and suppress baryogenesis. This effect is known as decoherence. These same processes also contribute to the diffusion of the particles within the plasma. Therefore, the diffusive mean free path λ which we calculate is the relevant parameter for estimating the supression due to decoherence.

In this work, we use the method described above to estimate the mean free path λ_s and the diffusion constant D_s of stops that have a soft supersymmetry breaking mass $m_s \sim T$ in the unbroken phase of the electroweak plasma. We use the same method to estimate the mean free path λ_q and the diffusion constant D_q for quarks and compare our values with those of Ref. [32]. We find that our method reproduces the results of Ref. [32] for the set of parameters used therein. In general, our results suggest that the values of λ and D of squarks are close to those of quarks.

In calculating λ and D, we consider only strong interactions, for they dominate the diffusion of squarks and quarks in the plasma. In the case of squarks, we further assume that scatterings from the heavy gluinos and squarks do not contribute signif-

[1]Non-elastic processes in which the species of the particle changes do contribute to the mean free path; however, these are not considered to be diffusive processes here.

icantly, leaving only quarks and gluons as the dominant scatterers. As consideration of more scatterers can only decrease the calculated values of λ and therefore D, the inclusion of only quark scatterers will yield an upper bound and even a reasonable order of magnitude estimate for the size of the squark diffusion constant D_s, in light of the results of Ref. [53]. In computing D_q, to facilitate comparison, we follow Ref. [32] and only consider t-channel quark-quark scattering.

The longitudinal and transverse gluons develop different thermal masses m_g and m_t in the plasma, referred to as Debye and magnetic masses, respectively. These masses provide physical infrared cutoffs for the exchanged gluon momentum. To incorporate these effects, we separate the gluon propagator into transverse and longitudinal parts that in general have different thermal masses. Whereas m_g is calculable at one loop, m_t is not calculable perturbatively and is unknown. Hence, we will present our results for two representative values of m_t. Note that since the momenta exchanged in the processes we consider are of order T, the use of the hard thermal loop gluon propagator is not justified [54, 55].

In the next section, we describe our method for calculating the diffusion constant of particles in the plasma. In Section 5.3, we present our estimates for λ_s, D_s, λ_q, and D_q, followed by a discussion of our results.

5.2 Calculation of the Mean Free Path and the Diffusion Constant

Let us consider a two body scattering process where the initial and final particles have 4-momenta (p, k) and (p', k'), respectively. We refer to each particle by its 4-momentum for the rest of this section. The p-particle, whose diffusion constant we calculate, scatters from the k-particle. For processes relevant to the calculation of the diffusion constant D, the final state p'-particle is of the same species as the initial p-particle. The p-particle, k-particle, p'-particle, and k'-particle have thermal distributions ρ_p, ρ_k, $\rho_{p'}$, and $\rho_{k'}$, respectively. The density per unit volume of a

particle with 4-momentum p is given by $\rho_p\, d^3p/(2\pi)^3$.

The transition probability for the above process per unit volume and per unit time is

$$\eta = \frac{d^3p}{(2\pi)^3\, 2p^0}\frac{d^3k}{(2\pi)^3\, 2k^0}\frac{d^3p'}{(2\pi)^3\, 2p'^0}\frac{d^3k'}{(2\pi)^3\, 2k'^0}(2\pi)^4\delta^{(4)}(p+k-p'-k')|\mathcal{M}|^2$$

$$\times\rho_p\,\rho_k\,(1\pm\rho_{p'})\,(1\pm\rho_{k'}), \tag{5.1}$$

where $\mathcal{M}$ is the amplitude for the scattering, and $\pm$ is for final state bosons or fermions, respectively. Let $d\sigma$ be the differential cross section for this process,

$$d\sigma = \frac{d^3p'}{(2\pi)^3\, 2p'^0}\frac{d^3k'}{(2\pi)^3\, 2k'^0}(2\pi)^4\delta^{(4)}(p+k-p'-k')\frac{|\mathcal{M}|^2(1\pm\rho_{p'})(1\pm\rho_{k'})}{4\sqrt{(p\cdot k)^2-m_p^2\,m_k^2}}. \tag{5.2}$$

Comparing Eqs. (5.1) and (5.2) yields

$$\eta = \left[\frac{d^3p}{(2\pi)^3\,p^0}\right]\left[\frac{d^3k}{(2\pi)^3\,k^0}\right]\sqrt{(p\cdot k)^2-m_p^2\,m_k^2}\,\rho_p\,\rho_k\,d\sigma. \tag{5.3}$$

To get the rate of collision per unit time $\eta^{(1)}$ of one p-particle in the plasma, we divide η by $\rho_p\, d^3p/(2\pi)^3$, the volume density of p-particles:

$$\eta^{(1)} = \frac{d^3k}{(2\pi)^3\,p^0k^0}\sqrt{(p\cdot k)^2-m_p^2\,m_k^2}\,\rho_k\,d\sigma. \tag{5.4}$$

To calculate the mean free path associated with the above process, we need to find the total rate of collision per unit time $\eta^{(1)}_{tot}(p)$ for one particle with initial 4-momentum p into any final state in the allowed phase space, using the total cross section σ. From Eqs. (5.2) and (5.4) we get

$$\eta^{(1)}_{tot}(p) = \frac{2}{(4\pi)^5}\int\frac{d^3k}{p^0k^0}\int\frac{d^3p'd^3k'}{p'^0k'^0}\delta^{(4)}(p+k-p'-k')|\mathcal{M}|^2\,\rho_k(1\pm\rho_{p'})(1\pm\rho_{k'}). \tag{5.5}$$

Note that each scatterer included will give an additive contribution of this form to $\eta^{(1)}_{tot}$.

The collision time $\tau(p)$, the length of time between two successive collisions for a

p-particle, is the inverse of $\eta^{(1)}_{tot}(p)$

$$\tau(p) = \frac{1}{\eta^{(1)}_{tot}(p)}. \tag{5.6}$$

The distance $l(p)$ such a p-particle travels between two collisions is then given by $l(p) = (|\vec{p}|/p^0)\,\tau(p)$. We finally get the mean free path λ for the p-particle by taking the thermal average of $l(p)$, using the thermal distribution of the p-particles. We thus get

$$\lambda = \left[\int \frac{d^3p}{(2\pi)^3}\,\rho_p\right]^{-1} \int \frac{d^3p}{(2\pi)^3}\,\rho_p \frac{|\vec{p}|}{p^0\,\eta^{(1)}_{tot}(p)}\,, \tag{5.7}$$

where we have used Eq. (5.6). Note that this mean free path vanishes if the cross section suffers from infrared divergences. However, for diffusive processes, these divergences are suitably regulated and only processes with nontrivial momentum transfer contribute. The resulting mean free path (5.7) can then be related to the diffusion constant D by the relation

$$D = \frac{1}{3}\,\lambda\,\bar{v}, \tag{5.8}$$

where $\bar{v}$ is the mean velocity of the diffusing particle.

5.3 Results and Discussion

We begin this section by describing some of the thermal properties of gluons in the plasma and how we incorporate these properties into our calculations. Due to interactions with the plasma, gluons develop temperature dependent masses. The longitudinal gluons have a thermal Debye mass $m_g(T) = \sqrt{8\pi\alpha_s}\,T$ at the 1-loop level and the transverse gluons have a non-perturbative thermal magnetic mass $m_t(T)$ that is zero at the 1-loop level and is expected to be $\mathcal{O}(g_s^2\,T)$, where $\alpha_s = g_s^2/(4\,\pi)$. Thus, we may assume that the infrared screening of longitudinal gluons occurs at a momentum scale m_g, and the similar scale for the transverse gluons is likely lower. At the electroweak phase transition temperature $T_c \approx 100$ GeV, $\alpha_s \approx 0.1$ and $m_g \approx 1.6\,T$. Since the magnetic mass is unknown, the choice of transverse infrared momentum cutoff

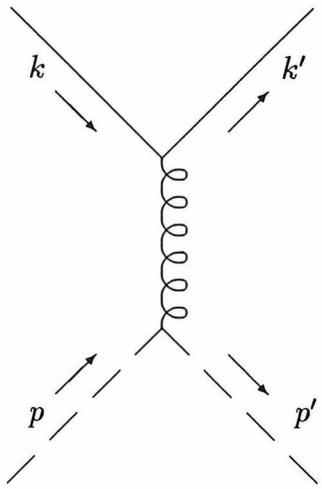

Figure 5.1: t-channel squark-quark Feynman diagram.

is rather arbitrary. However, because $g_s \approx 1$ at scale T_c, it is reasonable to assume that m_t is of order T. In Table 5.1, we take as two representative values $m_t = T$ and $m_t = m_g$.

The amplitude for the t-channel squark-quark diagram of Fig. 5.1 is

$$\mathcal{M}_{sq} = -8\pi\, \alpha_s\, T^a\, p^\mu D_{\mu\nu}\, \bar{q}(k')\, T^a \gamma^\nu q(k), \tag{5.9}$$

where T^a is a generator in the adjoint representation of the $SU(3)_c$ color gauge group, and q is a quark spinor. We work in the Landau gauge where, as explained in the supplementary Section 5.4, $(k'-k)^\mu D_{\mu\nu} = 0$. Since $p+p' = 2p+k-k'$, $\mathcal{M}_{sq}$ does not depend on p' explicitly. We use the amplitude $\mathcal{M}_{sq}$ of Eq. (5.9) to estimate the squark mean free path λ_s and diffusion constant D_s from Eqs. (5.7) and (5.8). The amplitude is squared and summed over all 72 species of quark scatterers (three colors, two spins, six flavors, and antiparticles). We have computed λ_s and D_s for supersymmetry breaking squark masses ranging from 50 GeV to 200 GeV and observed that their mass dependence is weak. These calculations were done using a c program which does the requisite five-dimensional integral. Our results are presented in Table 5.1,

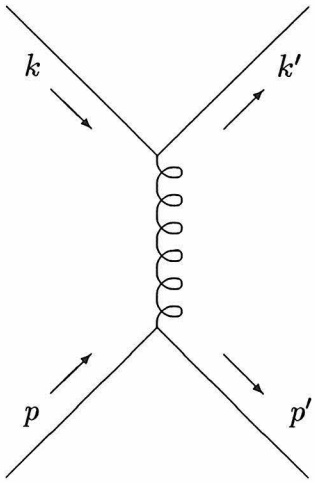

Figure 5.2: t-channel quark-quark Feynman diagram.

where the values of λ_s and D_s have been computed for $m_s = 100$ GeV.

In Ref. [32], D_q is computed using only the t-channel quark-quark scattering amplitude of Fig. 5.2, given by

$$\mathcal{M}_{qq} = -4\pi\,\alpha_s\,\bar{q}(p')\,T^a\gamma^\mu q(p)\,D_{\mu\nu}\,\bar{q}(k')\,T^a\gamma^\nu q(k). \tag{5.10}$$

To compare our method with that of Ref. [32], we have computed D_q, again numerically, using only $\mathcal{M}_{qq}$ (and again summing over 72 species of quark scatterers). The entries in Table 5.1 labeled "JPT" refer to the numbers we get for the set of parameters that are used in Ref. [32], namely $\alpha_s = 1/7$ and $m_g = m_t = \sqrt{8\pi\alpha_s}\,T = 1.9\,T$. We see that using the JPT parameters, we obtain the estimate $D_q \sim 6/T$ of Ref. [32], where only the leading logarithmic contributions were considered. Thus, our method independently reproduces the same result, suggesting that in our calculations the leading logarithmic contributions are dominant, although we do not isolate these contributions in computing our results. Therefore, we believe that our results are reliable at the level of leading logarithm calculations, and are good up to factors of order unity. Note that we do not consider all the processes that contribute at

	α_s	m_g	m_t	λ	D	Remarks
quark	1/10	$1.6T$	$1.0T$	$13/T$	$4/T$	
	1/10	$1.6T$	$1.6T$	$24/T$	$8/T$	
	1/7	$1.9T$	$1.9T$	$18/T$	$6/T$	JPT
squark	1/10	$1.6T$	$1.0T$	$12/T$	$3/T$	
$m_s = 100$ GeV	1/10	$1.6T$	$1.6T$	$18/T$	$5/T$	
	1/7	$1.9T$	$1.9T$	$14/T$	$4/T$	JPT

Table 5.1: Results for λ and D

this level: scatterings from on-shell gluons in the plasma also provide a substantial contribution. However, the results of Ref. [53] suggest that the inclusion of these diagrams will not change the results by more than a factor of 2.

Our calculations suggest that $\lambda_s \approx \lambda_q$ and $D_s \approx D_q$, up to factors of order unity, and most likely to within 30%. For $m_t = T < m_g$, we get $\lambda \lesssim 10/T$ and $D \lesssim 3/T$. On the other hand, if $m_t = m_g$, our results increase by about a factor of 2.

5.4 Thermal Gluon Propagator

In this supplementary section, we give the expression we use for the approximate thermal gluon propagator in a plasma, taking the different properties of the longitudinal and transverse gluons into account as represented by their respective cutoffs m_g and m_t. Let $n^\mu = (1,0,0,0)$ be the 4-velocity of the plasma in the plasma frame. We denote the 4-momentum q of the propagating gluon by $q^\mu = (q^0, \vec{q})$ in the plasma frame. The component of n that is orthogonal to q is given by $\tilde{n}$, where

$$\tilde{n}^\mu = n^\mu - \frac{(n \cdot q)q^\mu}{q^2}. \tag{5.11}$$

We define two projection operators $P_{\mu\nu}$ and $Q_{\mu\nu}$, where

$$P_{\mu\nu} = g_{\mu\nu} - \frac{q_\mu q_\nu}{q^2} - \frac{\tilde{n}_\mu \tilde{n}_\nu}{\tilde{n}^2} \tag{5.12}$$

and

$$Q_{\mu\nu} = \frac{\tilde{n}_\mu \tilde{n}_\nu}{\tilde{n}^2}. \tag{5.13}$$

The expression for the Landau gauge thermal gluon propagator in our approximation is then given by

$$D_{\mu\nu}^{(L)} = -\left[\frac{1}{q_T^2}P_{\mu\nu} + \frac{1}{q_L^2}Q_{\mu\nu}\right], \tag{5.14}$$

where $q_T^2 = q^2 - m_t^2$ and $q_L^2 = q^2 - m_g^2$, and from $q^\mu P_{\mu\nu} = q^\mu Q_{\mu\nu} = 0$, we have $q^\mu D_{\mu\nu}^{(L)} = 0$.

Chapter 6 Conclusions

This initial work on scalar baryon number transport baryogenesis [33] presented in Chapter 4 provides only a rough estimate of the baryon density produced as it is only intended to show the viability of the mechanism. It accomplished this goal, showing that squarks can contribute to baryogenesis at a level comparable to the quark contribution. One of the weakest areas of the analysis was the lack of knowledge of the squark diffusion constant; the work [45] presented in Chapter 5 addressed this weakness. There are other facets of the mechanism which require polishing. This is true of the axial transport mechanism as well.

The biggest uncertainty for any baryogenesis mechanism is that the character of the phase transition remains in doubt. The experimental determination of the multiplicity of Higgs and their masses and couplings would go a long way towards improving this area of knowledge. There are improvements to be made in calculation of phase transition parameters from this data, as well [17]. In addition to the order of the phase transition and its strength, it is necessary to pin down the wall velocity and profile (especially its width) as well as the relative magnitudes of the order parameters for the various Higgs fields and how they change across the bubble walls.

The method used to take into account the decoherence caused by the gluon scattering was admittedly very crude. This also must be improved. A more refined method was used to determine the baryon density produced by axial transport [25] which takes into account the effects of gluon scattering more physically. It would be desirable to use this method, suitably augmented, to analyze scalar baryon number transport.

Ultimately, the success or failure of the mechanism will be determined by experiment. Only if squarks are found and their properties (masses, couplings, and CP violating phases) are measured, can it be determined whether they make a significant contribution to baryogenesis. Whether it is squarks or quarks, or neither, that

contribute the most to baryogenesis, within the next few decades the question of whether baryogenesis occurred at the electroweak phase transition will probably have been settled by experiment. If the answer is positive, it will represent another grand integration between astronomy and physics.

Bibliography

[1] A. Rand, *Introduction to Objectivist Epistemology*, Meridian Books, 1990.

[2] G. Hull, *Integration as the Dynamo of Reason*, Lyceum Seminars, 1994.

[3] I. Newton, *Philosophiae Naturalis Principia Mathematica*, Harvard University Press, 1972.

[4] A. Einstein, *The Meaning of Relativity*, Princeton University Press, 1956.

[5] A. D. Sakharov, *JETP Lett.* **5**, 24 (1967).

[6] M. Yoshimura, *Phys. Rev. Lett.* **41**, 281 (1978); (Errata) **42**, 746 (1978).

[7] R. H. Brandenberger and A.-C. Davis, *Phys. Lett.* **B308**, 79 (1993);
R. H. Brandenberger, hep-ph/9702217.

[8] D. A. Kirzhnits and A. D. Linde, *Ann. Phys.* **101**, 195 (1976);
L. Dolan and R. Jackiw, *Phys. Rev.* D9, 3320 (1974);
M. Sher, *Phys. Rep.* **179**, 273 (1989).

[9] M. Dine, P. Huet, R. G. Leigh, A. Linde and D. Linde, *Phys. Rev.* **D46**, 550 (1992).

[10] P. Arnold and O. Espinosa, *Phys. Rev.* **D47**, 3546 (1993);
Z. Fodor and A. Hebecker, *Nucl. Phys.* **B432**, 127 (1994).

[11] C. Rebbi, *Lattice Gauge Theories and Monte Carlo Simulations* (World Scientific, Singapore, 1983);
K. Jansen, *Nucl. Phys.* **B47**, 196 (1996).

[12] K. Funakubo, Prog. Theor. Phys. **96**, 475 (1996).

[13] G. D. Moore and T. Prokopec, *Phys. Rev. Lett.* **75**, 777 (1995); *Phys. Rev.* **D52**, 7182 (1995).

[14] B. Liu, L. McLerran and N. Turok, *Phys. Rev.* **D46**, 2668 (1992).

[15] N. S. Manton, *Phys. Rev.* **D28**, 2019 (1983);
F. R. Klinkhamer and N. S. Manton, *Phys. Rev.* **D30**, 2212 (1984).

[16] M. E. Shaposhnikov, *JETP Lett.* **44**, 465 (1986); *Nucl. Phys.* **B287**, 757 (1987);
A. I. Bochkarev and M. E. Shaposhnikov *Mod. Phys. Lett.* **A2**, 417 (1987).

[17] M. Carena, M. Quirós and C. E. M. Wagner, Phys. Lett. **B380**, 81 (1996);
D. Delepine, J.-M. Gerard, R. Gonzalez Felipe and J. Weyers, *Phys. Lett.* **B386**, 183 (1996);
B. de Carlos and J. R. Espinosa, hep-ph/9703212.

[18] P. Arnold, D. T. Son and L. G. Yaffe, *Phys. Rev.* **D55**, 6264 (1997);
P. Huet and D. T. Son, *Phys. Lett.* **B393**, 94 (1997).

[19] G. D. Moore, C. Hu and B. Muller, hep-ph/9710436.

[20] J. S. Bell and R. Jackiw, *Nuovo Cimento* **60A**, 47 (1969);
S. L. Adler, *Phys. Rev.* **117**, 2426 (1969).

[21] G. 't Hooft, *Phys. Rev. Lett.* **37**, 8 (1976).

[22] G. R. Farrar and M. E. Shaposhnikov, *Phys. Rev. Lett.* **70**, 2833 (1993); *Phys. Rev* **D50**, 774 (1994); hep-ph/9406387.

[23] M. B. Gavela, P. Hernández, J. Orloff and O. Pène, *Mod. Phys. Lett.* **A9**, 795 (1994); M. B. Gavela, M. Lozano, J. Orloff and O. Pène *Nucl. Phys.* **B430**, 345 (1994);
M. B. Gavela, P. Hernández, J. Orloff, O. Pène and C. Quimbay *Nucl. Phys.* **B430**, 382 (1994);
P. Huet and E. Sather *Phys. Rev.* **D51**, 379 (1995).

[24] A. G. Cohen and A. E. Nelson, *Phys. Lett.* **B297**, 111 (1992).

[25] P. Huet and A. E. Nelson, *Phys. Lett.* **B355**, 229 (1995); *Phys. Rev.* **D53**, 4578 (1996).

[26] M. Carena, M. Quiros, A. Riotto, I. Vilja and C. E. M. Wagner, hep-ph/9702409.

[27] M. Aoki, N. Oshimo and A. Sugamoto, hep-ph/9612225;
M. Aoki, A. Sugamoto and N. Oshimo, hep-ph/9706287.

[28] M. P. Worah, hep-ph/9702423; hep-ph/9704389.

[29] E. Kolb and M. Turner, *The Early Universe*, Addison-Wesley (1990).

[30] G. Steigman, *Ann. Rev. Astron. Astrophys.* **14**, 339 (1976).

[31] C. J. Copi, D. N. Schramm and M. S. Turner, *Phys. Rev. Lett.* **75**, 3981 (1995).

[32] M. Joyce, T. Prokopec and N. Turok, *Phys. Lett.*, **B338**, 269 (1994); **B339**, 312 (1994); *Phys. Rev.* **D53**, 2930 (1996); *ibid.* 2958.

[33] H. Davoudiasl, K. Rajagopal and E. Westphal, *Nucl. Phys* **B515**, 1 (1998).

[34] C. Adloff *et al.*, H1 Collaboration, *Z. Phys.* **C74**, 191 (1997);
J. Breitweg *et al.*, Zeus Collaboration, *Z. Phys.* **C74**, 207 (1997).

[35] A. G. Cohen, D. B. Kaplan and A. E. Nelson, *Phys. Lett.* **B245**, 561 (1990); *Nucl. Phys.* **B349**, 727 (1991).

[36] A. E. Nelson, D. B. Kaplan and A. G. Cohen, *Nucl. Phys.* **B373**, 453 (1992);
A. G. Cohen, D. B. Kaplan and A. E. Nelson, *Phys. Lett.* **B294**, 57 (1992); **B336**, 41 (1994).

[37] G. F. Giudice and M. E. Shaposhnikov, *Phys. Lett.* **B326**, 118 (1994).

[38] G. Moore, hep-ph/9705248.

[39] A. G. Cohen, D. B. Kaplan and A. E. Nelson, *Phys. Lett.* **B388**,588 (1996).

[40] L. Alvarez-Gaumé, J. Polchinski and M. B. Wise, *Nucl. Phys.* **B221**, 495 (1983); J. Ellis and S. Rudaz, *Phys. Lett.* **B128**, 248 (1983).

[41] T. Falk, K. A. Olive and M. Srednicki, *Phys. Lett.* **B354**, 99 (1995); T. Falk and K. A. Olive, Phys. Lett. **B375**, 196 (1996).

[42] T. Multamäki and I. Vilja, hep-ph/9705469.

[43] M. Quiros, hep-ph/9703326.

[44] W. Buchmüller and D. Wyler, *Phys. Lett.* **B121**, 321 (1983); J. Polchinski and M. B. Wise, *Phys. Lett.* **B125**, 393 (1983).

[45] H. Davoudiasl and E. Westphal, hep-ph/9802355.

[46] V. A. Rubakov and M. E. Shaposhnikov, *Phys. Usp.* **39**, 461 (1996).

[47] N. Turok and J. Zadrozny, *Phys. Rev. Lett.* **65**, 2331 (1990); *Nucl. Phys.* **B358**, 471 (1991); L. McLerran, M. Shaposhnikov, N. Turok and M. Voloshin, *Phys. Lett.* **B256**, 451 (1991).

[48] M. Dine, P. Huet, R. Singleton Jr. and L. Susskind, *Phys. Lett.* **B257**, 351 (1991); M. Dine, P. Huet and R. Singleton Jr., *Nucl. Phys.* **B375**, 625 (1992).

[49] A. G. Cohen, D. B. Kaplan and A. E. Nelson, *Phys. Lett.* **B263**, 86 (1991); M. Dine and S. Thomas, *Phys. Lett.* **B328**, 73 (1994).

[50] A. Lue, K. Rajagopal and M. Trodden, *Phys. Rev.* **D56**, 1250 (1997).

[51] K. S. Babu, C. Kolda, J. March-Russell and F. Wilczek, hep-ph/9703299.

[52] S. Wolfram, *Mathematica*, 3rd ed. (Wolfram Media/Cambridge University Press, 1996).

[53] G. D. Moore and T. Prokopec, *Phys. Rev.* **D52**, 7182 (1995).

[54] H. A. Weldon, *Phys. Rev.* **D26**, 1394.

[55] E. Braaten and R. D. Pisarski, *Phys. Rev.* **D42**, 2156;

E. Braaten and R. D. Pisarski, *Nucl. Phys.* **B337**, 568.

A. Riotto, Phys. Rev. **D53**, 5834 (1996).

P. Hernández and N. Rius, *Nucl. Phys.* **B495**, 57 (1997).